Aggregation behavior of non-symmetrically end-capped thermo-responsive block copolymers in aqueous solution: between polymer coil and micellar state

Albert Prause[a,‡], Michelle Hechenbichler[b,‡], Benjamin von Lospichl[a,†], Artem Feoktystov[d], Ralf Schweins[e], Najet Mahmoudi[f], André Laschewsky[b,c,] and Michael Gradzielski[a,]**

[a] Technische Universität Berlin, FG Physical Chemistry/ Molecular Material Science, Straße des 17. Juni 135, 10623 Berlin, Germany

[b] Department of Chemistry, Universität Potsdam, Karl-Liebknecht-Straße 24–25, 14476, Potsdam, Germany

[c] Fraunhofer Institute of Applied Polymer Research IAP, Geiselbergstraße 69, 14476 Potsdam, Germany

[d] Forschungszentrum Jülich GmbH, Jülich Centre for Neutron Science JCNS at Heinz Maier–Leibnitz Zentrum MLZ, Lichtenbergstraße 1, 85748 Garching, Germany

[e] Institut Laue–Langevin, DS/ LSS, 71 Avenue des Martyrs, CS 20 156, F-38042 Grenoble Cedex 9, France

[f] ISIS Facility, STFC, Rutherford Appleton Laboratory, Harwell Campus, Didcot OX11 0QX, UK

KEYWORDS

RAFT synthesis, self-assembly, thermo-responsive, light scattering, small-angle neutron scattering

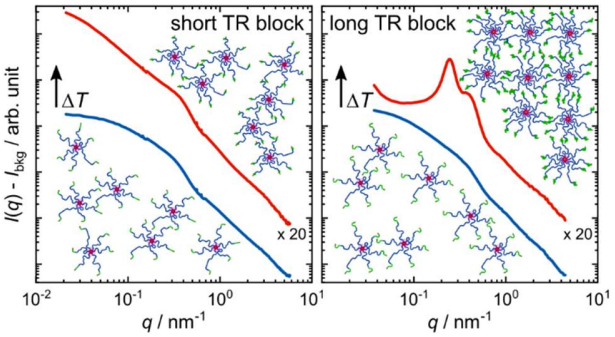

For Table of Contents Only

ABSTRACT

The thermo-sensitive aggregation behavior in aqueous solution of a library of amphiphilic BAB* copolymers is studied where ”A” represents a long permanently hydrophilic poly(*N*,*N*-dimethylacrylamide) (pDMAm) block, ‘B’ a permanently hydrophobic end with a *n*-dodecyl chain, and ”B*” a thermo-responsive (TR) block featuring a lower critical solution temperature (LCST). Four polyacrylamides are employed for B*, namely poly(*N*-*n*-propylacrylamide) (pNPAm), poly(*N*-isopropylacrylamide) (pNiPAm), poly(*N*,*N*-diethylacrylamide) (pDEAm), and poly(*N*-acryloylpyrrolidine) (pNAP), which differ with respect to the hydrophilicity of their amide side chains and LCST behavior. While blocks A and B were kept constant, the lengths of the TR blocks were varied systematically. These amphiphilic copolymers were studied as a function of concentration and temperature via light and neutron scattering (SLS, DLS, SANS). For sufficiently long pNiPAM and pDEAm blocks ($DP_n > 40$), a pronounced hydrophobic effect at temperatures above the LCST transition results in well-structured, ordered aggregates. Thus, the aggregation can be controlled by choice and length of the TR block, thereby elucidating a so far hardly explored class of temperature-sensitive polymeric amphiphiles.

INTRODUCTION

Building smart, adaptive systems has received much attention during the past decade. For this area of research, materials need to be developed which exhibit a controlled response to external stimuli. A class of such smart materials are amphiphilic block copolymers, which change their structure in solution as a function of such a stimulus, where this change may be particularly large for the case of self-assembling copolymers. Such systems are widely used, for instance, to control rheological properties [1] of a solution, or the ability to solubilize or release active agents.[2–4] Modern synthesis methods increasingly enable the tuning of the properties by tailoring the molecular structure and architecture. Hence, hydrophobically modified (HM) block-copolymers which are also thermo-responsive (TR) can precisely be designed. The architecture of the resulting HMTR polymers directly affects the self-assembly and thereby their rheological properties in solution. When thermo-responsive behavior is implemented in such HMTR polymers, the responsive blocks typically exhibit a lower critical solution temperature (LCST) in aqueous solution. This enables the switching of the TR block between being hydrophilic or hydrophobic in nature as a function of temperature, i.e., below the LCST-transition the TR block is fully solvated, in an extended conformation and flexible, whereas above the LCST-transition, the block is largely desolvated, and in a collapsed state, thereby inducing or modulating aggregation phenomena, such as the formation of polymer micelles.[5,6] This phenomenon has been exploited extensively in the past, the most intensely studied thermo-responsive polymer being poly(*N*-isopropylacrylamide) (pNiPAm), with an LCST around 32 °C.[7–9] Still, a plethora of alternative polymers exists, which provide a large choice of different transition temperatures and behaviors.[10,11]

Polymers for rheological control are typically designed as symmetrical triblock copolymers BAB with a long hydrophilic center block (A) and two identical short hydrophobic end blocks (B)

(Scheme 1a).[12,13] In a temperature-sensitive version, either the A (Scheme 1b) or the B blocks (Schema 1c) can switch their character from hydrophilic to hydrophobic upon a thermal stimulus, or vice versa. In this work, we synthesize non-symmetrical architectures BAB*, in which the long inner A block is permanently hydrophilic and framed by a small permanently hydrophobic end group B ('hydrophobic sticker') on one end, but a different hydrophobic end block B* on the other end. The latter is only conditionally hydrophobic and designed to exhibit an LCST transition in water (Scheme 1d). It might be noted here that previously we had studied telechelic polymers with permanently hydrophobic long alkyl chains as end-caps connected by a different number of arms of hydrophilic poly(*N*,*N*-dimethylacrylamide) (pDMAm), where the formation of flower-like micelles and interconnected micellar networks was observed in dependence on the number of arms and concentration.[14,15]

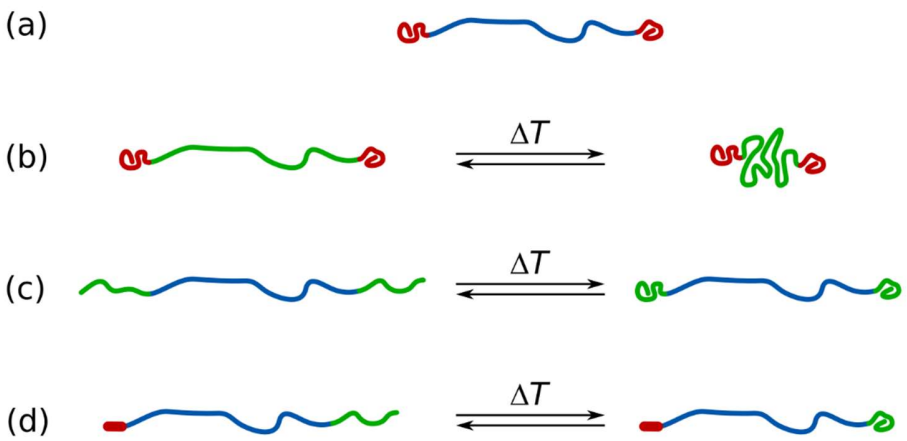

Scheme 1. Architectures of hydrophobically modified thermo-responsive (HMTR) block copolymers: (a) conventional design with permanently hydrophilic and hydrophobic blocks, (b) conventional design with responsive (hydrophilic/hydrophobic) central block, (c) conventional design with two responsive (hydrophilic/hydrophobic) end blocks, (d) investigated design with

one permanent and one responsive (hydrophilic/hydrophobic) block (red: hydrophobic block, green: responsive block, blue: hydrophilic block).

In analogy to previous studies by our groups,[14–17] the permanently hydrophilic central block of the copolymers is built from the nonionic monomer *N*,*N*-dimethylacrylamide (**1**, DMAm, Figure 1) throughout this study, whose polymers are known to be highly hydrophilic within the full temperature range of liquid water under atmospheric pressure.[18] The hydrophobic sticker group consisting of a *n*-dodecyl (C_{12}) chain attached to an aromatic residue (R-group) is kept constant and is conceived to correspond structurally to a low molar mass surfactant. In contrast, the responsive end block is varied by employing four different acrylamide monomers, namely *N*-*n*-propylacrylamide (**2**,NPAm), *N*-isopropylacrylamide (**3**, NiPAm), *N*,*N*-diethylacrylamide (**4**, DEAm), and *N*-acryloylpyrrolidine (**5**, NAP) whose homopolymers are known for increasing LCST values in aqueous solution between 20 and 60 °C (see Figure 1).[10,11] Moreover, this study follows a preliminary one on HMTR polymers of this particular design, which used poly(*N,N*-bis(2-methoxyethyl)acrylamide) as thermo-responsive block, resulting however in transition temperatures that were unpractically high.[19]

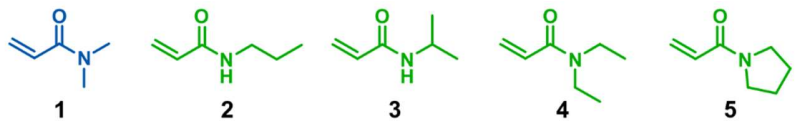

Figure 1. Monomers used for synthesizing the HMTR block copolymers. The permanently hydrophilic first block is made of monomer *N*,*N*-dimethylacrylamide (**1**, DMAm, in blue). The thermo-responsive blocks with LCST behavior (in green) are made from monomers *N*-*n*-propylacrylamide (**2**, NPAm, LCST(pNPAm) ≈ 22 °C [20]), *N*-isopropylacrylamide (**3**, NiPAm,

LCST(pNiPAm) ≈ 32 °C [9]), *N*,*N*-diethylacrylamide (**4**, DEAm, LCST(pDEAm) ≈ 30 °C [21]), and *N*-acryloylpyrrolidine (**5**, NAP, LCST(pNAP) ≈ 55 °C [20,22]).

EXPERIMENTAL METHODS

Chemicals

The reagents and solvents used are specified in the Supporting Information. Monomer *N*,*N*-dimethylacrylamide (**1**, DMAm, ≥ 99.0 % stabilized with 4-methoxyphenol 'MEHQ', TCI Deutschland GmbH, Eschborn, Germany) was distilled under reduced pressure prior to use (1 mbar, b. p. < 80 °C). The synthesis of monomer *N*-*n*-propylacrylamide (**2**, NPAm) was adapted from reported procedures,[23] and is described in detail in the Supporting Information (SI). Monomer *N*-isopropylacrylamide (**3**, NiPAm, > 98 %, stabilized with MEHQ, TCI) was purified by repeated crystallization from *n*-heptane prior to use. Monomer *N*,*N*-diethylacrylamide (**4**, DEAm, ≥ 99.8 % stabilized with MEHQ, TCI) was distilled prior to use. The synthesis of monomer *N*-acryloylpyrrolidine (**5**, NAP) was adapted from reported procedures,[22,24] as described in detail in the Supporting Information. The synthesis of the chain transfer agent 4-(*n*-dodecylcarbamoyl)benzyl-3-(trimethylsilyl)propyl)carbonotrithioate (**6**, CTA1) is described elsewhere.[19] Deionized water was further purified by a Millipore Milli-Q Plus water purification system (Merck Millipore, Darmstadt, Germany), resistivity 18.2 MΩ cm. D_2O (99.9 % D content, Deutero GmbH, Kastellaun, Germany), was filtered through membrane filters (0.22 μm, cellulose acetate) before use.

Polymer synthesis

The preparation of the hydrophobically modified (HM) homo- and block-copolymers followed the same procedures. Homopolymer synthesis is exemplified for $\mathbf{C_{12}DMAm_{168}}$ in the following:

monomer DMAm (17.5 mL, 16.9 g, 0.170 mol, 202 eq.), initiator V-40 (20.6 mg, 0.0843 mmol, 0.1 eq.) and CTA **6** (442.6 mg, 0.8415 mmol, 1 eq.) were dissolved in benzene (76 mL). The solution was purged with argon for 45 min and immersed into a preheated oil bath with a temperature of 90 °C. After stirring for 3 h, the reaction was stopped by opening the flask to the air and cooling with liquid nitrogen. The polymer was isolated and purified by two subsequent precipitations into diethyl ether. The polymer was dried in a vacuum oven, dissolved in distilled water and lyophilized. The polymer yield was 10.98 g (63 %) with a theoretical number average degree of polymerization of $DP_n = 168$ (calculated as the employed molar ratio of monomer to RAFT chain transfer agent multiplied by the monomer conversion, approximating the monomer conversion by the polymer yield).

Block copolymers were prepared employing RAFT-made pDMAm samples as macro chain transfer agent (macroCTA), as exemplified for the polymerization of NiPAm: pDMAm (1.03 g, 0.050 mmol) and NiPAm (226.9 mg, 2.01 mmol, 40 eq.) were dissolved in benzene (5.1 mL), and 0.61 mL of a stock solution of initiator V-40 in benzene (2 g L^{-1}) were added (equivalent to 0.0050 mmol, 0.1 eq. of macroCTA). The mixture was purged with argon for 40 min, immersed into a preheated oil bath of a temperature of 90 °C, and stirred for 4 h. The reaction was stopped by opening the flask to the air and cooling with liquid nitrogen. The block copolymer was isolated and purified by analog to the homopolymer, by two subsequent precipitations into diethyl ether, drying in vacuo, dissolving in distilled water and lyophilization. The polymer yield was 1.03 g (82 %).

Size exclusion chromatography

All polymers were analyzed by size exclusion chromatography (SEC) with simultaneous UV and RI detection at room temperature (flow rate 0.5 mL min^{-1}). The eluent was

N-methyl-2-pyrrolidone (NMP) with 0.1 % LiBr. The stationary phase used was a 300 × 8 mm^2 PSS GRAM linear M column (7 µm particle size). Samples were filtered through 0.45 µm filters and the injected volume was 100 µL. Narrowly distributed polystyrene standards (PSS, Mainz, Germany) were used for calibration.

UV-vis spectroscopy

UV-vis spectra were recorded on a Perkin Elmer Lambda 25 UV-vis Spectrometer, using a quartz cuvette with 1.0 cm path length. Number average molar masses M_n^{UV} were calculated by end-group analysis, using the absorbance *E* at 309 nm of the π-π* transition of the trithiocarbonate chromophore of the Z-group in methanol (cf. Figure S2). Values were calculated according to $M_n^{UV} = \varepsilon \cdot c_g \cdot d \cdot E^{-1}$ where ε is the molar extinction coefficient ([ε] = L mol^{-1} cm^{-1}), c is the concentration of the polymer in solution ([c_g] = g L^{-1}), and *d* is the optical path length ([*d*] = cm). The molar extinction coefficient ε of the trithiocarbonate chromophore was assumed to be 15800 L mol^{-1} cm^{-1} at 307 nm in methanol, as determined for the structurally similar trithiocarbonate reference *N*,*N*-dimethyl-2-(((butylthio)carbonothioyl)thio)propionamide.[25]

Sample preparation

The stock solutions were prepared by weighing the HMTR polymer in a vial and adding the needed amount of solvent (Milli-Q water or filtered D_2O) to get the desired concentration, mostly 55 g L^{-1}. The sample solutions for each polymer were prepared from the 55 g L^{-1} stock solution by dilution with the solvent (Milli-Q water or filtered D_2O). All samples were prepared in terms of weight fractions by using a balance. Thus, the samples were exactly described via a weight fraction. The samples were labeled according to their mass concentrations in g L^{-1} rounded to two significant figures. Thus, the precision of the prepared sample concentrations is higher than given and typically the uncertainty is well below 1 %.

For the scattering experiments (neutron and light scattering) the samples were prepared with filtered D_2O.

Turbidimetry

The temperature dependent transmission was measured with a Cary 5000 spectrometer (Varian), applying heating and cooling rates of 0.5 K min^{-1}. Temperatures are precise within 0.5 K. The cloud point is determined as the temperature onset of the decay of the transmission curve.

Visual analysis

A visual analysis of photographs taken from samples at different temperatures was carried out with a Python based script. The photographs were converted to gray scale and the scale was adjusted such that the background was set to a value of 0 and the sample holder (made from acrylic) to a value of 255. The background and the sample holder were not moved while taking all photos to ensure reliable reference points. After this the gray values were taken from the middle of the cuvette and averaged vertically. The recorded gray values refer basically to the scattering of light at ~90°.

Light scattering

Static (SLS) and dynamic (DLS) light scattering were performed with a 3DSpectrometer apparatus (LSinstruments, Switzerland). The instrument is equipped with a He-Ne laser ($\lambda = 632.8$ nm) and all measurements were carried out with an angle scan (2θ) between 30 and 135° in 5° steps and a temperature ramp from 20 to 60 °C in 5 °C steps. At each angle three repetitions were performed with a duration of 60 s.

The static intensity was deduced according to $I^{\mathrm{SLS}}_{\mathrm{sample}}(q) = \frac{C_{\mathrm{n,sample}} - C_{\mathrm{n,solvent}}}{C_{\mathrm{n,toluene}}} \cdot R_{\mathrm{toluene}}$, where $q = \frac{4\pi n_0}{\lambda} \sin\left(\frac{2\theta}{2}\right)$ is the magnitude of the scattering vector, $C_{\mathrm{n},i} = \frac{C_i}{P_i}$ is the count rate C divided

by the laser power P of species i and $R_{\text{toluene}} = 1.37 \cdot 10^{-5}\ \text{cm}^{-1}$ is the Rayleigh ratio of toluene for the given laser wavelength at 25 °C.[26] For calculating the effective molecular weight of the aggregates and the corresponding effective aggregation number, $I(0)$ is needed and was estimated via the Guinier law, Equation 1, in the q-range of 0.0066–0.0128 nm^{-1} (30–60°).

$$I(q) = I(0) \cdot \exp\left(-R_{\text{g}}^2 q^2/3\right) \tag{1}$$

The effective aggregation number ($N_{\text{eff}}^{\text{SLS}}$) from the obtained $I(0)$ values was estimated via

$$N_{\text{eff}}^{\text{SLS}} = \frac{I(0)}{K \cdot c_g \cdot M_{\text{n}}^{\text{theo}} \cdot Đ} \tag{2}$$

with $K = \frac{4\pi^2 n_0^2}{N_{\text{A}} \lambda^4} \left(\text{d}n/\text{d}c_g\right)^2$, where K is the optical constant, c_g the mass concentration of polymer in solution, $M_{\text{n}}^{\text{theo}}$ and $Đ$ are the molecular weight and dispersity of the individual polymers, respectively (see Table 1), n_0 the refractive index of the solvent, $\text{d}n/\text{d}c_g$ the refractive index increment for the polymer in solution and N_{A} the Avogadro constant. The $\text{d}n/\text{d}c_g$ values were determined experimentally with an Orange Analytics 19" dn/dc instrument and the obtained values are given in Table S2.

The dynamic light scattering data were analyzed based on the optimized regularization techniques (ORT) at an angle of 90°, which yields a distribution of the correlation times.[27,28] The analysis was performed with SimplightQt [29] (Python based in-house software for analyzing light scattering data). For details see SI. In summary, we derived from it the distribution of diffusion coefficients D that can be converted to the distribution of apparent hydrodynamic radii $R_{\text{h}}^{\text{app}}$ via the Stokes-Einstein equation, $R_{\text{h}}^{\text{app}} = k_B T/(6\pi\eta_0 D)$, where k_{B} is the Boltzmann constant, T the absolute temperature and η_0 the solvent viscosity.

Small-angle neutron scattering

The small-angle neutron scattering (SANS) experiments were performed at *Heinz Maier–Leibnitz Zentrum* (MLZ, Garching, Germany), at *Institut Laue–Langevin* (ILL, Grenoble, France), and at ISIS Pulsed Neutron Source (STFC Rutherford Appleton Laboratory, Didcot, U.K.) on the SANS instruments KWS-1,[30,31] D33,[32] and ZOOM,[33] respectively. In the experiments a q-range was covered of 0.018–4.0 nm^{-1} (KWS-1), 0.025–5.8 nm^{-1} (D33), and 0.038–7.2 nm^{-1} (ZOOM). Further information can be found in the Supporting Information (SI). The samples were measured in a temperature-controlled sample changer using Hellma QS cells with 2 mm path length. The sample temperatures were 25/50 °C at KWS-1, 25/56 °C at D33, and 25/55 °C at ZOOM. The data reduction and scaling to absolute scale was done with QtiKWS [34] at KWS-1, LAMP [35] at D33, and Mantid [36] at ZOOM.

The characterization of the polymer chain structure in solution was conducted in the high q regime above 1.5 nm^{-1} where the scattering intensity is mainly related to the polymer chain scattering. For the analysis, the polymer coil model with excluded volume effects [37] was employed (Equations S1–S3 in the SI). The radius of gyration ($R_\mathrm{g} \equiv \langle R_\mathrm{g}^2 \rangle^{1/2}$) and the mass fractal dimension (f_p) were obtained and used for further analysis of the scattering data. The best-fit values are listed in Tables S3 and S4. For further considerations, R_g was converted to an end-to-end distance ($R_\mathrm{ee} \equiv \langle R_\mathrm{ee}^2 \rangle^{1/2}$, via $R_\mathrm{ee} = \left(6R_\mathrm{g}^2\right)^{1/2}$, which is strictly speaking only valid for a Gaussian coil).

From the SANS data an effective aggregation number was estimated by extrapolation to q = 0. The Guinier law (cf. Equation 1) was used. The q-range was set individually for each polymer between 0.03 and 0.3 nm^{-1}, where the data mostly exhibit an approximately linear regime. The fits are shown in Figures S15–S17. An effective aggregation number $N_\mathrm{eff}^\mathrm{SANS}$ was calculated from the intensity $I(0)$ as

$$N_{\mathrm{eff}}^{\mathrm{SANS}} = \frac{M_{\mathrm{eff}}^{\mathrm{SANS}}}{M_{\mathrm{n}}^{\mathrm{theo}} \cdot Đ} = \frac{I(0)}{M_{\mathrm{n}}^{\mathrm{theo}} \cdot Đ \cdot K^{\mathrm{SANS}} \cdot c_{\mathrm{g}}} \quad (3)$$

where c_g is the mass concentration, $I(0)$ the estimated forward scattering of the Guinier fit, and $K^{\mathrm{SANS}} = \left(SLD_{\mathrm{sol}} - SLD_{\mathrm{p}}\right)^2 / \left({\rho_{\mathrm{p}}}^2 N_{\mathrm{A}}\right)$ ([K^{SANS}] = mol cm^2 g^{-2}) the SANS contrast factor with SLD_{sol} as scattering length density of the solvent, SLD_{p} as scattering length density of the dry polymer, ρ_{p} as mass density of the dry polymer based on partial volumes of the building blocks (see Table S1 and S2), and M_n^{theo} and $Đ$ are the molecular weight and dispersity of the individual polymers, respectively (see Table 1). The dispersity was considered due to the fact that $M_{\mathrm{eff}}^{\mathrm{SANS}}$ is a mass averaged molecular weight. It must be noted that the influence of a structure factor was not considered for the Guinier analysis.

The scattering model, based on established models,[38–40] considers the aggregation of N_{agg} polymer chains into spherical micelles, described with the micellar form factor $P_{\mathrm{mic}}(q)$, and the agglomeration of N_{clu} micelles into pearl-necklace-like clusters.

$$I(q) = \frac{\phi}{V_{\mathrm{mic}}} \cdot \left[S_{\mathrm{clu}}(q) P_{\mathrm{mic}}(q)\right] \cdot S_{\mathrm{hs}}^{\mathrm{eff}}(q) + I_{\mathrm{bkg}} \quad (4)$$

where ϕ is the dry volume fraction of the dissolved polymer, V_{mic} $(= N_{\mathrm{agg}} \cdot V_{\mathrm{p}})$ the dry volume of the micelle, V_{p} the volume of a polymer chain, N_{agg} the aggregation number, $S_{\mathrm{clu}}(q)$ the form factor for a pearl-necklace chain [41] consisting of N_{clu} pearls directly attached to each other, $S_{\mathrm{hs}}^{\mathrm{eff}}(q)$ the effective hard-sphere structure factor, and I_{bkg} the incoherent background.

The model intensity $I(q)$ is smeared for each configuration separately according to the uncertainty in the magnitude of the scattering vectors σ_q. Further details are reported in the SI and published elsewhere.[42]

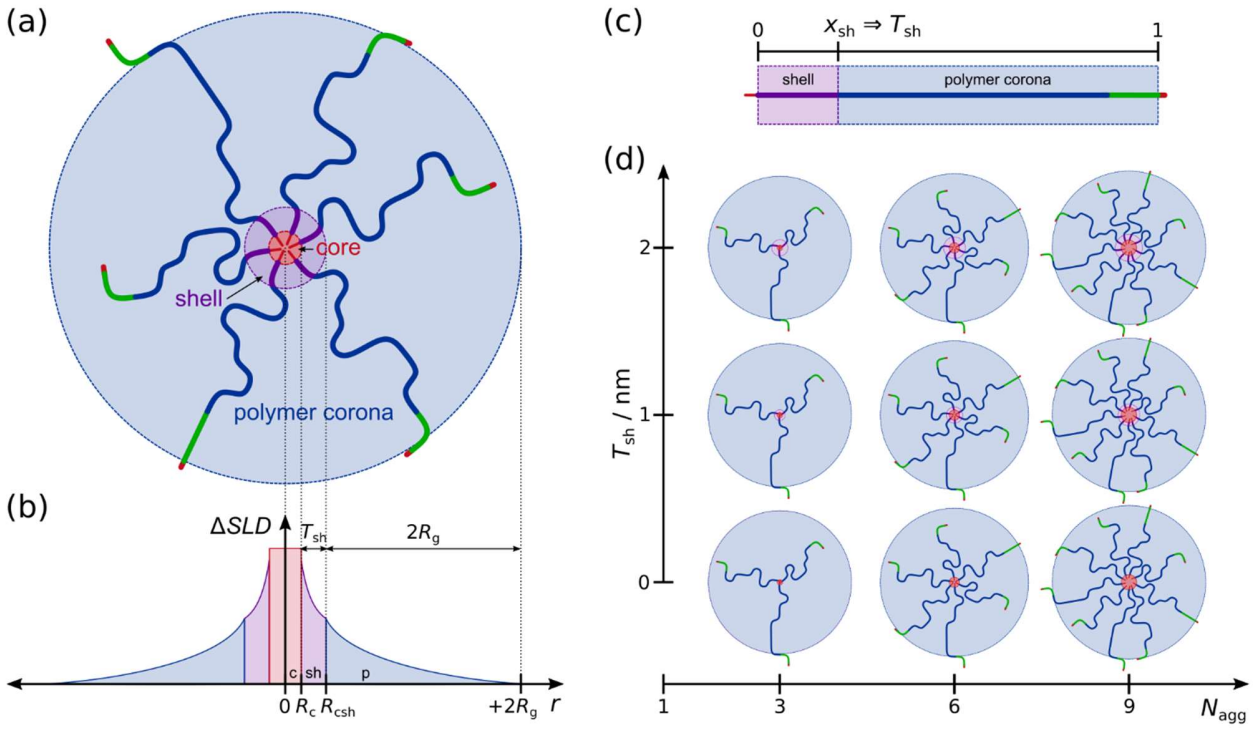

Scheme 2. (a) Schematic drawing of a polymer micelle described by the micellar form factor $P_{\mathrm{mic}}(q)$ (Equation 5). (b) Scattering length density (*SLD*) profile of the polymer micelle with the three segments, core (red, c), shell (purple, sh), and polymer corona (blue, p) consisting of the hydrophobic R-groups, the fraction x_{sh} of polymer chains in the shell, and the remaining fraction of each polymer chain represented as polymer coils, respectively. The total micellar radius is defined as $R_{\mathrm{mic}} = R_{\mathrm{csh}} + 2R_{\mathrm{g}}$ with $R_{\mathrm{csh}} = R_{\mathrm{c}} + T_{\mathrm{sh}}$. (c) Representation of the fraction x_{sh} which translates into a shell thickness T_{sh}. (d) Sketched polymer micelles show different aggregations numbers (N_{agg}) and shell thicknesses T_{sh} resulting from x_{sh}.

The micellar form factor, $P_{\mathrm{mic}}(q)$, is adapted from J. S. Pedersen and C. Gerstenberg (1996),[43] B. Hammouda and M. H. Kim (2017),[40] and summarized by Y. Wei and M. Hore (2021).[39] It describes the formation of a spherical core containing the hydrophobic tails while the headgroups

are rendered as polymer coils. In addition, an exponentially decaying shell was added to describe the denser region adjacent to the core based on the idea of T. Zinn *et al.* (2017).[38] For this case $P_{\mathrm{mic}}(q)$ is written as:

$$P_{\mathrm{mic}}(q) = P_{\mathrm{csh}}(q) + N_{\mathrm{agg}}P_{\mathrm{p}}(q) + 2N_{\mathrm{agg}}^2 X_{\mathrm{csh-p}}(q) + N_{\mathrm{agg}}\big(N_{\mathrm{agg}} - 1\big)X_{\mathrm{p-p}}(q) \qquad (5)$$

where $P_{\mathrm{csh}}(q)$ is the core-shell form factor, N_{agg} the aggregation number of polymer chains, $P_{\mathrm{p}}(q)$ the polymer coil form factor, $X_{\mathrm{csh-}}\ (q)$ the core-shell–polymer interference term and $X_{\mathrm{p-p}}(q)$ the polymer–polymer interference term.

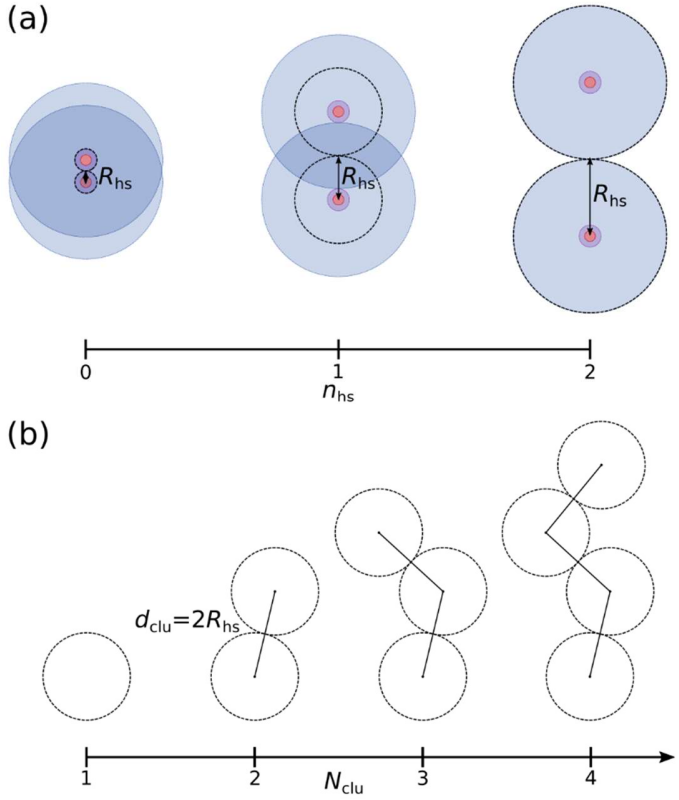

Scheme 3. (a) Hard-sphere interaction of polymer micelles within the defined boundaries of $0.0 \leq n_{\mathrm{hs}} \leq 2.0$ ($R_{\mathrm{hs}} = R_{\mathrm{csh}} + n_{\mathrm{hs}}R_{\mathrm{g}}$) which allows for a penetration of the polymer corona. (b) Representation of the pearl-necklace-like clustering of polymer micelles with a micellar distance of $d_{\mathrm{clu}} = 2R_{\mathrm{hs}}$.

The clustering of micelles is considered in terms of a pearl-necklace chain form factor which accounts for the correlation of pearls along the necklace chain.[38,41] The pearls are directly attached to each other whereby no connecting rods are considered.

$$S_{\mathrm{clu}}(q) = (1 - p_{\mathrm{clu}}) \cdot S_N(q, \lfloor N_{\mathrm{clu}} \rfloor) + p_{\mathrm{clu}} \cdot S_N(q, \lfloor N_{\mathrm{clu}} \rfloor + 1) \tag{6}$$

with

$$S_N(q, N) = \frac{2}{N}\left[\frac{N}{1-j_0(qd_{\mathrm{clu}})} - \frac{N}{2} - \frac{1-j_0(qd_{\mathrm{clu}})^N}{\left(1-j_0(qd_{\mathrm{clu}})\right)^2} \cdot j_0(qd_{\mathrm{clu}})\right] \tag{7}$$

where $d_{\mathrm{clu}} = 2R_{\mathrm{hs}}$ is the distance between the micelles in the cluster (cf. Scheme 3a), $p_{\mathrm{clu}} = N_{\mathrm{clu}} - \lfloor N_{\mathrm{clu}} \rfloor$ the difference between number of micelles in the cluster and the corresponding rounded down integer $\lfloor N_{\mathrm{clu}} \rfloor$, and $j_0(x)$ the spherical Bessel function of 0$^{\mathrm{th}}$ order. Thus, $S_{\mathrm{clu}}(q)$ is a linear combination of the cluster sizes of $\lfloor N_{\mathrm{clu}} \rfloor$ and $\lfloor N_{\mathrm{clu}} \rfloor + 1$ weighted by p_{clu}. Equation 7 was derived by W. Burchardt and K. Kajiwara (1970)[44] to describe a freely jointed chain. Due to the use of a freely jointed chain describing the clustering process, the excluded volume of the polymer micelles is not considered. Therefore, the applied hard-sphere structure factor is based on the total number density of polymer micelles interacting with the hard-sphere radius.

The hard-sphere structure factor according to the Percus–Yevick approximation [45] describes the spacial interaction of polymer micelles and is given by

$$S_{\mathrm{hs}}(q) = \frac{1}{1+24\phi_{\mathrm{hs}} \cdot \frac{G(A)}{A}} \tag{8}$$

where $A = 2qR_{\mathrm{hs}}$ and

$$G(A) = \frac{a}{A^2}[\sin(A) - A \cdot \cos(A)] + \frac{b}{A^3}[2A \cdot \sin(A) + (1 - A^2) \cdot \cos(A) - 2] + \frac{c}{A^5}[-A^4 \cdot \cos(A) + 4([3A^2 - 6] \cdot \cos(A) + [A^3 - 6A] \cdot \sin(A) + 6)],$$

$$a = \frac{(1+2\phi_{\mathrm{hs}})^2}{(1-\phi_{\mathrm{hs}})^4},\ b = \frac{-6\phi_{\mathrm{hs}}\left(1+\frac{\phi_{\mathrm{hs}}}{2}\right)^2}{(1-\phi_{\mathrm{hs}})^4},\ c = \frac{\frac{\phi_{\mathrm{hs}}}{2}(1+2\phi_{\mathrm{hs}})^2}{(1-\phi_{\mathrm{hs}})^4}. \tag{9}$$

The hard-sphere radius R_{hs} and volume fraction ϕ_{hs} are expressed in terms of micellar dimensions $R_{\mathrm{hs}} = R_{\mathrm{csh}} + n_{\mathrm{hs}} R_{\mathrm{g}}$, where $0 \leq n_{\mathrm{hs}} \leq 2$ which allows for interpenetration of micelles, and $\phi_{\mathrm{hs}} = {}^{1}N_{\mathrm{mic}} \cdot \frac{4}{3}\pi R_{\mathrm{hs}}^3$ with ${}^{1}N_{\mathrm{mic}} (= \phi / V_{\mathrm{mic}})$ as number density of polymer micelles (cf. Scheme 3a). This relation cannot be imposed for the highest concentrations (> 50 g L^{-1}) and for samples phase-separating at higher temperature because of the large extent of interpenetration and additional attractive interactions – and then it was treated as an additional parameter.

Following the decoupling approach, an effective hard-sphere structure factor $S_{\mathrm{hs}}^{\mathrm{eff}}(q)$ is defined as

$$S_{\mathrm{hs}}^{\mathrm{eff}}(q) = 1 + \beta(q) \cdot (S_{\mathrm{hs}}(q) - 1) \tag{10}$$

where $\beta(q) = A_{\mathrm{mic}}(q)^2 / P_{\mathrm{mic}}(q)$ is the quotient of the squared micellar scattering amplitude $A_{\mathrm{mic}}(q)^2$ and the micellar form factor $P_{\mathrm{mic}}(q)$.

The developed polymer micelle scattering model is used with basically 4 free parameters, i.e., the aggregation number N_{agg}, the fraction of polymer chains in the shell x_{sh}, the number N_{clu} of micelles forming a pearl-necklace-like cluster, and the hard-sphere radius R_{hs}, which is varied via n_{hs}. Only for the above-mentioned cases (high concentrations, > 50 g L^{-1}, and samples phase-separating at higher temperature), the hard-sphere volume fraction ϕ_{hs} becomes a free parameter in the boundaries of the dry volume fraction ϕ and a volume fraction of 0.494 at which a phase transition of hard-sphere occurs.[46] The best-fit values are listed in Tables S6 and S7. Further details and the influence of each parameter on the scattering intensity (Figure S19) can be found in the SI.

RESULTS AND DISCUSSION

Polymer synthesis

The amphiphilic block copolymers were synthesized by the RAFT method,[47] which allows for controlling the block lengths, minimizes the polymer dispersities *Đ*, and enables the stable attachment of the hydrophobic sticker group (cf. Scheme 1). The block copolymers were prepared by two consecutive RAFT polymerizations, employing a chain transfer agent (CTA), in which both the leaving group (the so-called Z-group) and the re-initiation group (the so-called R-group) were specifically functionalized. The trithiocarbonate CTA **6** (Figure 2) introduces a hydrophobic end group featuring a *n*-dodecyl chain to the block copolymers via the R-group, thereby assuring its attachment to the HMTR polymer by a hydrolytically inert carbon-carbon bond. This is a distinct advantage over most of the reported hydrophobized RAFT agents, where the hydrophobic group is part of the Z-group, which is quite sensitive to hydrolysis.[48–50] CTA **6** bears a trimethylsilyl (TMS) moiety in the Z-group that is a powerful ^{1}H NMR label (see Figure S3), as its signal appears close to 0 ppm in the spectra, a region free of signals for most polymers and solvents. The intense singlet signal of the TMS group disposing of 9 protons facilitates the determination of the number average molar mass by end group analysis.[51,52] Moreover, it also enables the estimation of the end group fidelity by comparing the integrals of Z- and R-group signals, whose aromatic protons appearing around 8 ppm are also well-resolved.[19]

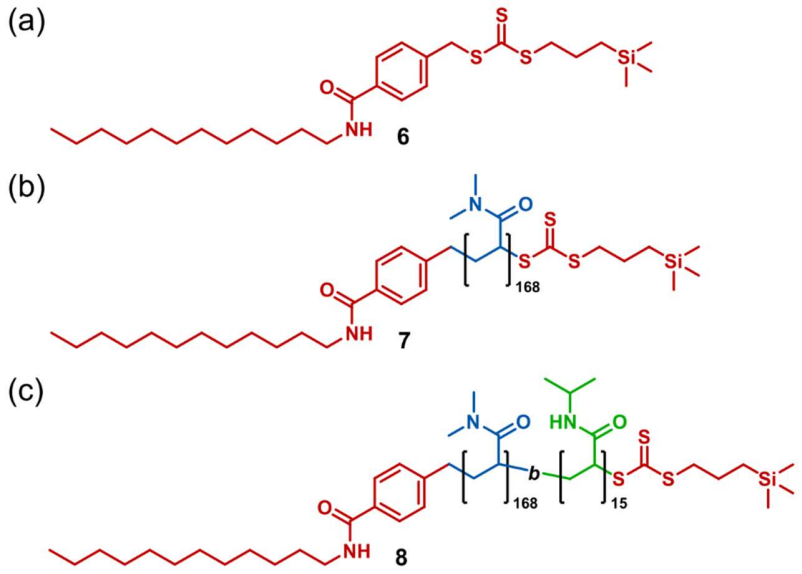

Figure 2. Overview of the three steps in RAFT polymerization. (a) Chain-transfer agent (**6**) with *n*-dodecyl chain (C_{12}) for hydrophobic modification, (b) hydrophobically modified (HM) pDMAm homopolymer (**7**, **C_{12}DMAm$_{168}$**) and (c) exemplarily HMTR pDMAm-*b*-pNiPAm block copolymer (**8**, **C_{12}DMAm$_{168}$NiPAm$_{15}$**). The number of monomer units refers to the theoretically calculated number based on the yield (red: hydrophobic part, green: LCST block, blue: hydrophilic block).

The analysis of the ^{1}H NMR spectra of homopolymer **C_{12}DMAm$_{168}$** (**7**) that served as macroCTA in the second RAFT polymerization step, indicated indeed a high end group fidelity (Table 1), due to the low ratio [CTA]:[initiator] of 10:1 engaged and the high conversion of DMAm reached after only 3 h. This was crucial for introducing reliably the additional thermo-responsive polymer block. All block copolymers are characterized by rather narrow molar mass distributions with $Đ < 1.3$, and the molar masses determined by different methods match well with each other, indicating successfully controlled polymerizations (see Table 1). In the set of block copolymers prepared, the length of the permanently hydrophilic pDMAm block (A) was kept between 120 and 170 repeat units to assure sufficient solubility of the polymers even above the phase transition of

the thermo-responsive blocks. In any case, the hydrophilic chain must be long enough to be able to bridge aggregates for acting as effective associative thickener. Much shorter lengths were applied for the thermo-responsive block B* (cf. Scheme 1), ranging from 20 to 60 repeat units to study its influence on the phase transition behavior.

All polymers synthesized for this work are listed in Table 1, together with their relevant characteristics.

Table 1. Overview of synthesized polymers with degree of polymerization (DP_n^{NMR}), as obtained by NMR, of the pDMAm block and the corresponding TR block, the resulting molar mass (M_n), obtained from NMR, SEC, or UV-vis analysis. The degree of polymerization (DP_n^{theo}) refers to the theoretically calculated number with respect to the determined yield. Additional information is provided in Table S2 in the SI.

Polymers	$M_n^{theo\ (a)}$ / kg mol^{-1}	DP_n^{theo}	$M_n^{NMR\ (b)}$ / kg mol^{-1}	$DP_n^{NMR\ (b)}$	$M_n^{UV\ (c)}$ / kg mol^{-1}	$M_n^{SEC\ (d)}$ / g mol^{-1}	$Đ^{(e)}$
DMAm$_{187}$	18.9	187	21	208	20	19	1.18
C$_{12}$DMAm$_{168}$	17.1	168	22	213	19	18	1.25
C$_{12}$DMAm$_{127}$	13.1	127	16	157	14	14	1.18
C$_{12}$DMAm$_{168}$NiPAm$_{15}$	18.8	15 (f)	23	11 (f)	25	21	1.25
C$_{12}$DMAm$_{168}$NiPAm$_{33}$	20.8	33 (f)	25	34 (f)	25	22	1.26
C$_{12}$DMAm$_{127}$NiPAm$_{50}$	18.8	50 (f)	24	66 (f)	26	23	1.21
C$_{12}$DMAm$_{168}$DEAm$_{14}$	18.9	14 (f)	23	14 (f)	23	19	1.19
C$_{12}$DMAm$_{168}$DEAm$_{27}$	20.1	27 (f)	27	45 (f)	25	22	1.25
C$_{12}$DMAm$_{127}$DEAm$_{48}$	19.2	48 (f)	27	90 (f)	23	21	1.18
C$_{12}$DMAm$_{168}$NAP$_{16}$	19.1	16 (f)	24	18 (f)	32	21	1.16
C$_{12}$DMAm$_{168}$NAP$_{27}$	20.4	27 (f)	26	36 (f)	30	24	1.16
C$_{12}$DMAm$_{127}$NPAm$_{31}$	16.6	31 (f)	21	45 (f)	28	20	1.25

[a] for calculation, monomer conversion was approximated by the determined yield. [b] by end group analysis via ^{1}H NMR spectroscopy, using the trimethylsilyl signal of the CTA's Z-group. [c] by end group analysis via UV-spectroscopy in methanol, using the π-π* transition band at 309 nm of the C=S double bond of the CTA's Z-group. [d] from SEC (eluent 0.1 wt% LiBr in NMP, calibration with polystyrene standards). [e] dispersity M_w/M_n according to SEC data. [f] numbers refer to DP_n of the thermo-responsive B* block.

Phase transition behavior in aqueous solution

The thermo-responsive behavior of the block copolymers in aqueous solution was investigated by temperature dependent turbidimetry for different concentrations (see Figure 3). While pDMAm is soluble in water from 0 to 100 °C, high molecular weight homopolymers of NPAm, NiPAm, DEAm and NAP (see Figure 1) show typically LCST phase transitions around 22 °C,[20] 32 °C,[9] 30 °C,[21] and 55 °C,[20,22] respectively. Upon shortening the block length, the transition temperatures typically increase.[53,54] While no macroscopic phase transition was detected for the block-copolymers bearing very short thermo-responsive blocks with $DP_n < 20$, samples of **$C_{12}DMAm_{168}NiPAm_{33}$**, **$C_{12}DMAm_{168}DEAm_{27}$** as well as their longer homologues showed a strong decrease in transmission above their respective phase transition temperature. Compared to the values typically reported for the homopolymers pNiPAm and pDEAm, the phase transition temperature of the corresponding block-copolymers was strongly increased up to a temperature of 60 °C. This increase is only to a small part a consequence of the short lengths of the thermo-responsive blocks, but mainly attributed to the attached long hydrophilic pDMAm block and the resulting overall higher hydrophilicity of the copolymers, as observed before.[17,19,22,55,56]

The longer the thermo-responsive blocks become, the more their cloud points approach the ones of their respective homopolymers (Figure 3). Although the LCSTs of pNiPAm and pDEAm have virtually the same value of about 32 °C and 30 °C, respectively, we observe different behavior for the block copolymers. The cloud point of **$C_{12}DMAm_{127}NiPAm_{50}$** is around 38–39 °C, whereas the

one of **$C_{12}DMAm_{168}DEAm_{48}$** is at a more elevated temperature of around 43–45 °C (Figure 3).[a]The different LCST types of the thermo-responsive polymers, namely type I (Flory–Huggins-like) for pDEAm but type II for pNiPAm,[7,11] might explain this difference. **$C_{12}DMAm_{168}NAP_{27}$** did not show a clear phase transition up to a temperature of 80 °C even at concentrations of up to 5.0 g L^{-1}. The cloud point of the homopolymer pNAP, which also displays LCST behavior of type I, is already quite high with about 55 °C. Hence, it seems likely that the additional hydrophilic pDMAm block increases the cloud point so much further, so that it is no longer in the interesting temperature range for water. However, in contrast, the Z-group bearing the hydrophobic TMS group has a hydrophobic character (though much less than the surfactant-like R-group). As it is directly attached to the thermo-responsive block, it will decrease the phase transition temperature of the polymers, counteracting partially the effect of the hydrophilic block on the other end. When the Z-group was intentionally removed (cf. Scheme S1), the cloud point for **$C_{12}DMAm_{168}DEAm_{27}$** increased from 50 °C to 59 °C for a concentration of 5.0 g L^{-1} demonstrating a strong effect of the rather small hydrophobic end group directly attached to the responsive block on the cloud point (see Figure S1). Note that however for larger hydrophobic groups capable of forming separate domains in water, such as the sticker group, their effect on the phase transition temperature tends to vanish.[57,58]

[a] The samples for turbidimetry were prepared in H_2O. In contrast, the samples for light and neutron scattering were prepared in D_2O. For pNiPAm it is reported that in D_2O the cloud point slightly increases by less than 1 °C.[65,66]

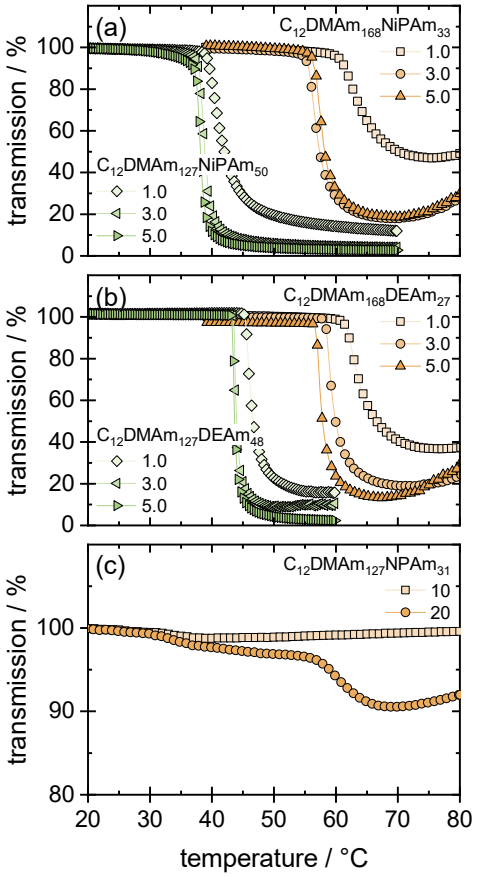

Figure 3. Temperature dependent turbidimetry (heating without stirring) as function of the polymer concentration of (a) **$C_{12}DMAm_{168}NiPAm_{33}$** and **$C_{12}DMAm_{127}NiPAm_{50}$**, (b) **$C_{12}DMAm_{168}DEAm_{27}$** and **$C_{12}DMAm_{127}DEAm_{48}$**, and (c) **$C_{12}DMAm_{127}NPAm_{31}$**. The concentrations are given in g L^{-1}.

Compared to the other copolymers, the block polymer **$C_{12}DMAm_{127}NPAm_{31}$** shows quite a different behavior in aqueous solution (Figure 3). Up to a concentration of 10 g L^{-1}, the transmission remains almost unchanged at ~100 %. However, for a concentration of 20 g L^{-1}, the transmission decreases by 9 % and an apparent two step transition is visible (Figure 3c). In the first step, the transmission starts to decrease softly at around 30°C, which is slightly higher than the phase transition temperature of 25 °C known for pNPAm.[59] Probably, this behavior is again

caused by the hydrophilic pDMAm block attached to the thermo-responsive block, elevating the phase transition temperature. In a second step, the transmission decreases more sharply, but after reaching a minimum at around 65 °C, it increases again. This two-step transition process also appeared in the cooling cycle (see Figure S4e) indicating stable aggregates undergoing a reversible aggregation process without any stirring of the system. Stable aggregates were also observed for block copolymers of poly(*N*-ethylacrylamide) (pNEAm) and pNPAm for different block lengths, even above the phase transition of ~70 °C of pNEAm though the block copolymers consist then only of water-insoluble (yet partially swollen) blocks.[52] However, when the block length ratio between the hydrophilic pNEAm and the collapsed pNPAm block was higher than 1:1, clusters were observed in transmission electron microscopy (TEM). The tendency towards cluster formation was explained by the still relatively short hydrophilic pNEAm block, which might not be sufficient to stabilize isolated micelles. Similarly, less turbid solutions were observed in the case of **$C_{12}DMAm_{127}NPAm_{31}$** where the pNPAm block is shorter than the hydrophilic pNEAm blocks used in the reference.

These findings suggest that not only the chemical structure of the thermo-responsive block and its length, but also the ratio between hydrophilic and hydrophobic block play an important role in the aggregation behavior of thermo-responsive block copolymers. Nevertheless, the hysteresis between heating and cooling is notable, which is typical for thermo-responsive polyacrylamides bearing NH groups like pNiPAm. These groups allow intramolecular hydrogen bonding between the amide groups in the collapsed state acting as physical crosslinking points, which must be unmade during the re-dissolution process.[60]

The thermo-responsive behavior is also summarized in Figure S5, where the visual appearance as observed after a waiting time of 15 min is reported in a quantitative way by analyzing the optical

appearance of the samples in the photographs. In general, the visual inspections confirm the results by turbidimetry (Figure 3) and extend these results to more concentrated samples. In particular, they confirm the observation of the uncommon behavior of the **$C_{12}DMAm_{127}NPAm_{31}$** with an additional transition taking place around 40 °C. That indicates a weaker tendency of the pNPAm block for association, which might be of a more dynamic nature than for the other HMTR blocks and correspondingly not lead to the marked turbidity seen there due to macroscopic phase separation.

Aggregation behavior in aqueous solution

Light scattering: First insights into the structure of the aqueous solutions of the different polymers as a function of concentration and temperature were gained via light scattering experiments. The static scattering intensity of the investigated HMTR block polymers for different concentrations is shown in Figure S6–S8 in the Supporting Information (SI) as a function of the magnitude of the scattering vector q. For further analysis, the low q data were fitted with the Guinier law (Equation 1) and the extrapolated forward scattering intensity $I(0)$ was converted into a molecular weight of the scattering objects. From this we calculated the effective aggregation number $N_{\mathrm{eff}}^{\mathrm{SLS}}$ (Equation 2), which is displayed in Figure 4 for different concentrations as a function of temperature. Interestingly, all HMTR polymers exhibit for all temperatures an effective aggregation number above 10. This fact does not necessarily imply that always proper micellar aggregation is observed here, as even for the homopolymer **$DMAm_{187}$** such a value is seen. However, it is likely the result of a network formation by entanglements, which is frequently observed in small-angle scattering of polymers.[61] In addition, it should be kept in mind that, due to the RAFT polymerization, even the homopolymer contains a hydrophobic moiety that may lead to enhanced association of entanglements.

The SANS data (discussed later in more detail in the SANS section) infer scattering patterns of single coils for **DMAm$_{187}$**, which clearly proves that here no compacted aggregation takes place, but a looser type of aggregation must be present. At low q, i.e., in the SLS q-range, a large upturn appears, thereby bing fully consistent with the SLS results. **DMAm$_{187}$** and the reference polymers without a TR block, i.e., **C$_{12}$DMAm$_{168}$** and **C$_{12}$DMAm$_{127}$**, show no significant temperature dependence in the observed temperature range, as expected due to the permanently hydrophilic character of the pDMAm block. Interestingly, **C$_{12}$DMAm$_{168}$** shows the most pronounced influence of the concentration, $N_{\mathrm{eff}}^{\mathrm{SLS}}$ decreases roughly by a factor of 4 between the concentrations of 5.9 and 23 g L^{-1}. This may be attributed to the effect of steric repulsion, as hydration of the hydrophilic block leads to a much higher effective volume fraction. This effect should be less pronounced for the less strongly hydrated TR blocks. In addition, they can offer more attractive interaction towards each other, which increases with rising temperature.

Most HMTR polymers with a short TR block (**C$_{12}$DMAm$_{168}$NiPAm$_{15}$**, **C$_{12}$DMAm$_{168}$NiPAm$_{33}$**, **C$_{12}$DMAm$_{168}$DEAm$_{14}$**, **C$_{12}$DMAm$_{168}$DEAm$_{27}$**, **C$_{12}$DMAm$_{168}$NAP$_{27}$**, **C$_{12}$DMAm$_{127}$NPAm$_{31}$**) show a slight increase of $N_{\mathrm{eff}}^{\mathrm{SLS}}$ with increasing temperature, but this increase is little affected by the concentration. Only for **C$_{12}$DMAm$_{168}$NAP$_{16}$**, the effective aggregation number $N_{\mathrm{eff}}^{\mathrm{SLS}}$ is initially relatively high with about 300, but then decreases systematically with rising temperature, especially above 45 °C. This observation is confirmed by DLS measurements shown in Figure S9c. Only HMTR polymers with longer TR blocks show a more pronounced temperature dependence, as seen before in the turbidity studies (Figures 3 and S5). In general, an increase of $N_{\mathrm{eff}}^{\mathrm{SLS}}$ with increasing temperature is observed for the various systems. Interestingly for the lower concentrations, **C$_{12}$DMAm$_{168}$NiPAm$_{33}$** and **C$_{12}$DMAm$_{168}$DEAm$_{27}$** show a more marked increase of $N_{\mathrm{eff}}^{\mathrm{SLS}}$ by more than one order of magnitude starting at 45 °C (see Figure 4c, 4d). The slight

decrease seen at 60 °C arises from the onset of phase separation of the sample. The same effect plays a major role at 22 g L^{-1}, where no direct increase of $N_{\mathrm{eff}}^{\mathrm{SLS}}$ is visible but the scatter of the intensity data becomes large due to being in the phase transition region.

The increase of $N_{\mathrm{eff}}^{\mathrm{SLS}}$ for **$C_{12}DMAm_{127}NiPAm_{50}$** and **$C_{12}DMAm_{127}DEAm_{48}$** is much more pronounced, increasing by more than two orders of magnitude in the temperature range of 35 and 40 °C. Obviously, such a length of the TR block, comprising about 50 repeat units, is required to impart strong responsiveness upon the temperature increase. Otherwise, in general the length of the TR block has little effect on $N_{\mathrm{eff}}^{\mathrm{SLS}}$, except for the case of NAP, where the longer block leads to substantially lower values of $N_{\mathrm{eff}}^{\mathrm{SLS}}$, while the shorter block shows the highest aggregation numbers. This might be attributed to the much higher LCST of pNAP. Thus, no phase transition is seen for both polymers **$C_{12}DMAm_{168}NAP_{16}$** and **$C_{12}DMAm_{168}NAP_{27}$** (see Figure S5a). Accordingly, the pNAP block acts primarily as a hydrophilic block and decreases the packing parameter with increasing length, thereby leading to formation of smaller micellar aggregates. Finally, for the HMTR polymer **$C_{12}DMAm_{127}NPAm_{31}$** at 5.6 g L^{-1}, a constant $N_{\mathrm{eff}}^{\mathrm{SLS}}$ value of about 20 is observed. Towards the higher concentrations, $N_{\mathrm{eff}}^{\mathrm{SLS}}$ increases notably above 30 °C from ~20 to ~50. This small transition coincides with the first step in the temperature dependent transmission curves of the 20 g L^{-1} solution visible in Figure 3c.

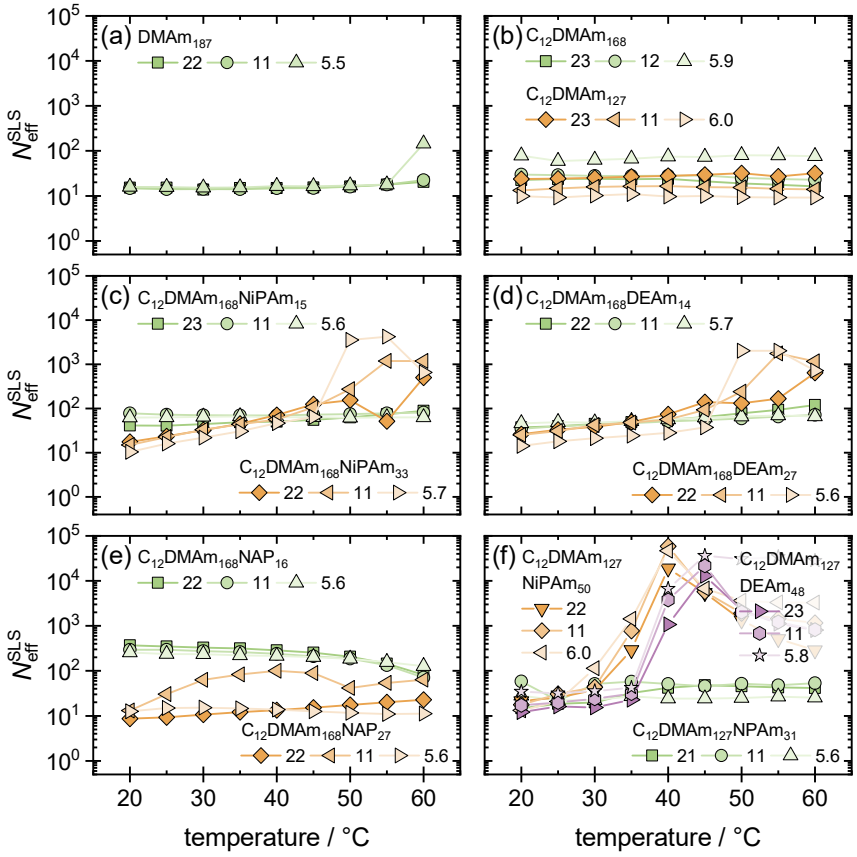

Figure 4. Effective aggregation number ($N_{\mathrm{eff}}^{\mathrm{SLS}}$) of HMTR polymers determined by static light scattering for the probed temperature range of 20–60 °C. According to Equation 2, $M_{\mathrm{n}}^{\mathrm{theo}}$ and $Đ$ were used as the molecular weight and dispersity for the corresponding HMTR polymers, respectively. Numbers in the labels refer to the mass concentration given in g L^{-1}. The estimated uncertainties are within the symbols.

The DLS autocorrelation curves generally show a relatively fast and rather monomodal decay (for a complete set see Figures S9–S11). Only for some cases, such as **$C_{12}DMAm_{168}NiPAm_{33}$** or **$C_{12}DMAm_{168}DEAm_{27}$**, a markedly slower decay of the autocorrelation function is observed. When analyzing the data by means of an optimized regularization technique (ORT) approach, this faster decay is always found to correspond to hydrodynamic radii of 10–25 nm as the dominant

component (for the complete set of data see Figures S12–S14). This size is in very good agreement with the expected size of micelles with a core formed by dodecyl chains and protruding hydrophilic chains with 170–200 monomer units. Upon heating to 55 °C, this main peak is shifted to a value of 80–100 nm for **$C_{12}DMAm_{127}NiPAm_{50}$** and **$C_{12}DMAm_{127}DEAm_{48}$** (Figure 5), thereby clearly revealing the temperature induced secondary aggregation of the primary copolymer aggregates. In contrast, a rising temperature has only a minor effect on the aggregate size of the hydrophobically modified pDMAm homopolymer system (Figures S12b and S14a). The same behavior is seen for the TR-copolymers with short TR blocks (Figures S12–S14).

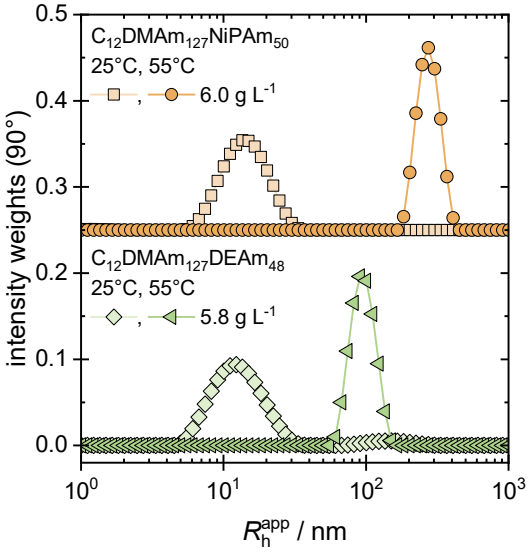

Figure 5. Exemplary intensity weighted size distributions of **$C_{12}DMAm_{127}NiPAm_{50}$** and **$C_{12}DMAm_{127}DEAm_{48}$** for the lowest concentration at 25 °C and 55 °C represented as weights of the underlying ORT analysis. The narrow distribution at 55 °C arises from the scattering above the LCST.

Small-angle neutron scattering (SANS): In order to deduce more detailed structural information, SANS experiments were performed for the different polymers as a function of

concentration and temperature. The complete set of SANS curves is shown in Figures S15–S17. Looking at the homopolymer **DMAm$_{187}$**, the scattering curve follows the expected pattern for individual polymer coils for high q but diverges for $q < 0.08$ nm^{-1} with a sudden upturn, which can be attributed to a network of entangled polymer chains (Figure 6a), as already seen by SLS. By dividing with the calculated intensity of polymer coils $I_{coil}(q)$ (Equation S1), we obtain an effective structure factor which is shown in Figure 6b. The effective structure factor exhibits a marked minimum S_{min}. This can be attributed to a correlation hole, i.e., an effective repulsion between the polymer chains, that becomes increasingly pronounced with increasing concentration (Figure 6c). In general, this effect is similarly seen for the other copolymers, as long as they do not yet aggregate significantly at higher temperature. This can be taken as evidence that in these situations, single copolymer chains are present and no aggregates.

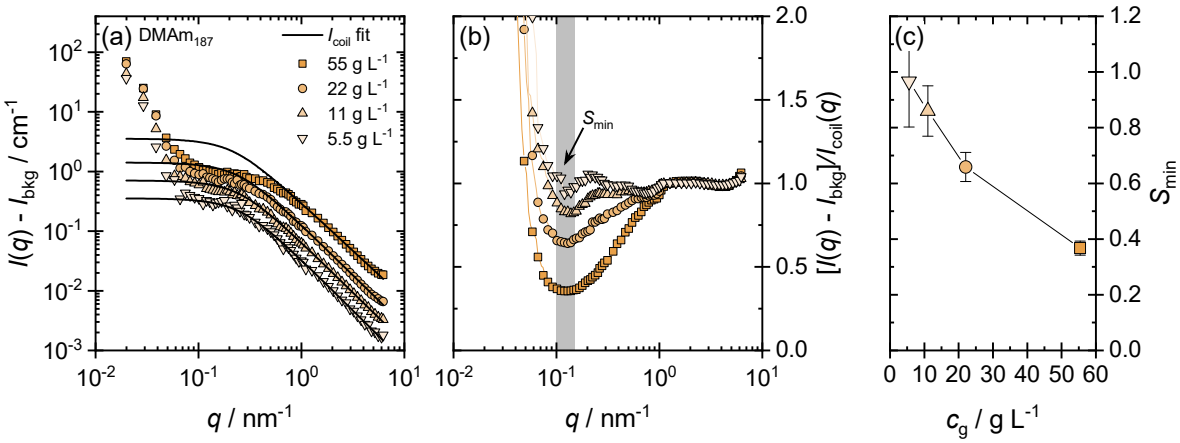

Figure 6. (a) Scattering curves of **DMAm$_{187}$** at 25 °C with the corresponding polymer coil model (see Equations S1–S3). The used molar weight M_n^{theo} and *SLD*s were taken from Table S2. (b) Effective structure factor where the minimum (S_{min}) is highlighted with a gray area. (c) S_{min} as the minimum of the effective structure factor curves (b) in the gray area plotted versus the mass concentration c_g.

For the simple hydrophobically modified polymer **C_{12}DMAm$_{168}$**, the scattering intensity at medium q (~ 0.1 nm^{-1}) scales simply with the concentration (Figure S15b). However, the scattering pattern changes systematically. Especially *at* the highest concentration of 56 g L^{-1}, it shows clearly the features of a globular structure (inset of Figure S15b). In contrast, at low concentration, the scattering curves are those of individual coils in solution. Upon raising the temperature from 25 to 50 °C, scattering intensity and aggregation only slightly increase (as similarly seen in SLS, Figure 4b). For **C_{12}DMAm$_{127}$** (see Figure S17a), a similar behavior is observed with the difference that somewhat larger aggregates are formed as indicated by the higher intensities in the mid and low q (see Figure S19). For the shorter hydrophilic block of **C_{12}DMAm$_{127}$**, a smaller head group area is expected at the amphiphilic interface. Following this, larger micelles are to be formed according to the packing parameter concept. In addition, at fixed mass concentration, this polymer contains a larger amount of C_{12} chains than its longer counterpart.

For the HMTR polymers, a short overview of the SANS patterns at low and high temperature is given in Figure 7a for the samples with ~22 g L^{-1}. It shows that for pNAP and pNPAm little temperature response is seen, while the response is very different for pDEAm and pNiPAm.

Looking in more detail at the HMTR polymers with a pNAP block, the scattering curves for different concentrations (Figures 7a and S15c and d) look very similar compared to their precursor homopolymer **C_{12}DMAm$_{168}$**. This implies that the pNAP block behaves similarly to the pDMAm block with respect to their hydrophilicity. At high temperature (55 °C), the intensity at low q is slightly increased compared to **C_{12}DMAm$_{168}$**, indicating a somewhat less repulsive interaction between the aggregates. For **C_{12}DMAm$_{168}$NAP$_{27}$**, the SANS intensity only increases slightly already in the range of 0.2–0.6 nm^{-1}. This indicates a smaller growth of aggregates without much further interconnection, in agreement with light scattering observations (Figure 4e). Apparently,

the LCST transition is shifted for pNAP copolymers to much higher temperatures so that effectively, the thermo-responsiveness is subdued in the useful temperature window and no real association takes place.

For the pNiPAm-containing HMTR polymers (Figure S16a and b), aggregation is somewhat higher than for the pure pDMAm systems already at 25 °C. Evidently, the less hydrophilic pNiPAm block favors aggregation. At higher temperature (50/56 °C), always a marked increase of scattering intensity is observed, i.e., increased aggregation or clustering. Only for **C_{12}DMAm$_{168}$NiPAm$_{33}$**, a very large increase is observed, which agrees with the light scattering results (Figure 4b). With increasing concentration up to 22 g L^{-1}, much larger interconnected structures are formed. Interestingly, the intensity at low q decreases again for the highest concentration of 56 g L^{-1} (Figure S16b). This indicates a more restricted interconnection of domains with a retained and somewhat more compacted local domain structure, and a much larger steric repulsion in the system.

For the pDEAm-based HMTR polymers, a very similar structural progression and temperature response is observed as for the pNiPAm systems. This suggests that the pDEAm and pNiPAm chains are very similar with respect to their hydrophobicity above the LCST, resulting in very similar structural reorganization and network formation (as seen in the low q upturn, especially visible for c_g = 22 g L^{-1}, see Figure 7a). Apparently, a minimum length of the LCST block of 20 monomer units is needed to induce a significant temperature response. As a consequence, substantial aggregation due to increased hydrophobic interaction at higher temperature is seen for **C_{12}DMAm$_{168}$NiPAm$_{33}$** and **C_{12}DMAm$_{168}$DEAm$_{27}$**, as evidenced by the increase of scattering intensity at low q.

Investigations on HMTR polymer samples with the shorter hydrophilic $DMAm_{127}$ block exhibit a generically similar aggregation behavior, but with a much more pronounced and different tendency for self-assembly at elevated temperature for the pNiPAm- and pDEAm-based systems. A very marked ordering effect upon increasing temperature is seen in the case of **$C_{12}DMAm_{127}DEAm_{48}$**, and to an even higher extent for **$C_{12}DMAm_{127}NiPAm_{50}$** (see Figure 7 and Figure S17). Sharp correlation peaks are noted already for the 6.0 g L^{-1} sample at 56 °C for **$C_{12}DMAm_{127}NiPAm_{50}$** (see Figure S17c), which indicate a repeat distance of the hydrophobic scattering domain of 35–40 nm with a high degree of ordering and more compacted hydrophobic domains. A somewhat larger spacing is observed for **$C_{12}DMAm_{127}DEAm_{48}$**, for which also the correlation peak is much broader, indicating a lower degree of ordering. Interestingly even for **$C_{12}DMAm_{127}NPAm_{31}$**, a weak ordering effect can be discerned (Figure S17b). This demonstrates that for **$C_{12}DMAm_{127}NPAm_{50}$** and **$C_{12}DMAm_{127}DEAm_{48}$**, a temperature induced self-assembly with a dense packing of compacted and ordered hydrophobic domains takes place. In Figure 7a this is contrasted to the cases of **$C_{12}DMAm_{168}NAP_{16}$** and **$C_{12}DMAm_{168}NiPAm_{15}$**, for which the temperature response is only very small, as similarly seen for the other copolymers bearing short hydrophobic blocks.

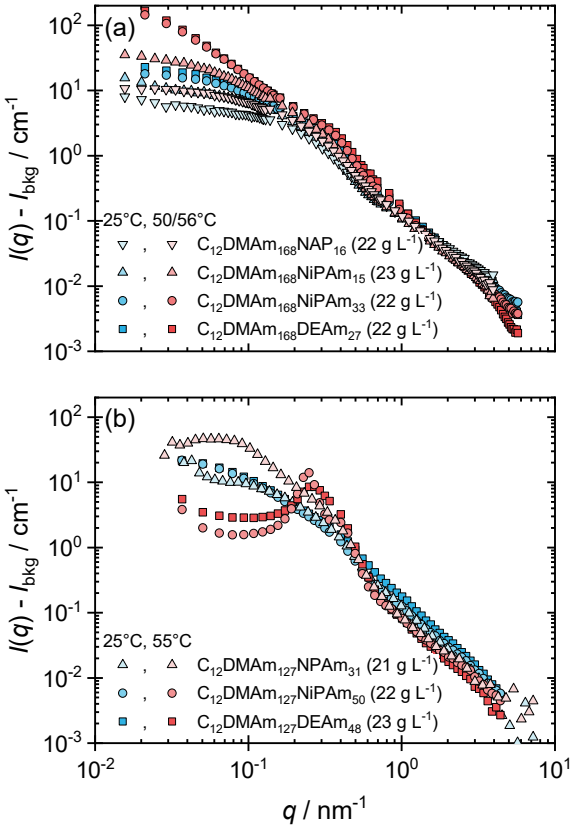

Figure 7. SANS intensity as a function of the modulus of the scattering vector q at 25 °C and 50/55/56 °C for: (a) **$C_{12}DMAm_{168}NAP_{16}$**, **$C_{12}DMAm_{168}NiPAm_{15}$**, **$C_{12}DMAm_{168}NiPAm_{33}$**, and **$C_{12}DMAm_{168}DEAm_{27}$** (longer hydrophilic block) and (b) **$C_{12}DMAm_{127}NPAm_{31}$**, **$C_{12}DMAm_{127}NiPAm_{50}$**, and **$C_{12}DMAm_{127}DEAm_{48}$** (shorter hydrophilic block).

A first analysis of the scattering data was performed to estimate the end-to-end distance R_{ee} and an effective aggregation number for the HMTR polymers. The end-to-end distance was estimated from the experimental data via fitting a polymer coil model with excluded volume effects with a given volume fraction and molecular weight of the polymers (Equations S1–S3 in the SI) in the high q regime above 1.5 nm^{-1}, using ($R_{ee} \approx \left(6\langle R_g^2\rangle\right)^{1/2}$), where R_g is the radius of gyration. The R_{ee} values are shown in Figure S18e–h.

The visible difference between the polymers **$C_{12}DMAm_{127}$** and **$C_{12}DMAm_{168}$** can be attributed to the difference of about 40 DMAm units in pDMAm block length. For the larger **$C_{12}DMAm_{168}$**, the end-to-end distance is roughly 2 nm longer than for shorter **$C_{12}DMAm_{127}$**. Most studied polymers exhibit basically no significant temperature dependency for the end-to-end distance, which is mainly governed by the permanently hydrophilic pDMAm block, and by little varying the length of the thermo-responsive block. Only the polymers **$C_{12}DMAm_{127}NiPAm_{50}$** and **$C_{12}DMAm_{127}DEAm_{48}$** show clearly higher R_{ee} values at 55 °C, which may be attributed to temperature-induced bridging of the formed hydrophobic domains. This suppresses backfolding of the chains, thereby explaining a larger extension of the chains.

The effective aggregation number N_{eff}^{SANS}, deduced from the intensity at $q = 0$ (fitting the intermediate q range of ~0.06-0.2 nm^{-1} with the Guinier law; for fits see Figures S15–S17), is shown in Figure S18a–d for all studied polymers except **$C_{12}DMAm_{127}NiPAm_{50}$** and **$C_{12}DMAm_{127}DEAm_{48}$** (here one sees marked structuring and as a result much reduced scattering at low q). For all polymers, N_{eff}^{SANS} increases basically with increasing concentration up to 22 g L^{-1}. Above this concentration, the influence of a structure factor, i.e., increasing steric repulsion, becomes significant that can be seen as a reduction of N_{eff}^{SANS} across all the studied polymers. The hydrophobically unmodified reference homopolymer **$DMAm_{187}$** forms basically no aggregates (cf. Figure 6 and as stated before the increase at still lower q can be attributed to the presence of an entanglement network). The HM homopolymers **$C_{12}DMAm_{168}$** and **$C_{12}DMAm_{127}$** have N_{eff}^{SANS} values up to 3 and 8, respectively. The pNAP systems behave very similar to **$C_{12}DMAm_{168}$** with higher values of N_{eff}^{SANS} up to 8. Further, no temperature effect is visible. Only the influence of a more prominent structure factor is noted again. The **$C_{12}DMAm_{127}NPAm_{31}$** behaves very similar to the precursor polymer **$C_{12}DMAm_{127}$** whereby the N_{eff}^{SANS} value increased to about 60 at the

higher temperature of 55°C (the lower value at 54 g L^{-1} arises from repulsive interactions seen here). For the other polymers, containing pNiPAm and pDEAm, in general we observe also low aggregation numbers in the range of 5 to 20. Similar trends are seen in light scattering (Figure 4). $N_{\mathrm{eff}}^{\mathrm{SANS}}$ is always higher at the higher temperature of 50/56 °C, and the difference becomes larger the longer the pNiPAm or pDEAm block is. At 25 °C, $N_{\mathrm{eff}}^{\mathrm{SANS}}$ is between 5 and 20 for a concentration up to 22 g L^{-1}, and increases to 20–50 at 50/56 °C.

In the next step, the clustered polymer micelle model (described in the Methods section and summarized in Equation 4) was used to quantify further the SANS data analysis of the studied polymers. In this model, we assume that micellar entities of an average aggregation number N_{agg} can be linked to form pearl-necklace-like clusters described by the number of micelles contained (N_{clu}), where the individual micelles interact via the excluded volume based on an effective hard-sphere radius R_{hs}. The parameter x_{sh} describes the polymer chain fraction in the shell which is much more condensed due to the proximity to the hydrophobic core. The remaining part of the polymer chains are dissolved in a corona that is described by their radius of gyration, R_{g}. The corresponding fits of the SANS data are displayed in Figures S21–S23 in the SI. The fit parameters and related parameters are shown in Figure S24 for the polymer micelle form factor, and in Figure S25 for the parameters for the pearl-necklace form factor and hard-sphere structure factor. For the polymer micelle form factor, the additionally given core radius R_{c} and shell thickness T_{sh}, arise directly from the fit parameters N_{agg} and x_{sh}, respectively. They were calculated to get a further structural picture of the micelles. The extra structure factor parameters, hard-sphere radius R_{hs} and hard-sphere volume fraction ϕ_{hs}, are directly linked to the variable parameter n_{hs} and were displayed for better comparability. For few samples marked with a prime or asterisk in Figure S25, ϕ_{hs} was used as a variable parameter, as described in the paragraph of the scattering model.

As already discussed, the simple homopolymer **DMAm$_{187}$** behaves like single coils and its R_g value is rather constant at 5–6 nm over the whole concentration range. In contrast, for the hydrophobically modified pDMAm homopolymers without a TR block, **C$_{12}$DMAm$_{168}$** and **C$_{12}$DMAm$_{127}$**, the mean aggregation number increases with concentration. N_{agg} starts at about 2 at 25 °C and levels off just below 6 and 9 at 50/55 °C, respectively. The radius of gyration is somewhat higher compared to that of the pDMAm homopolymer, as expected for a micellar aggregate. Due to the absence of a TR block, no clustering is expected to take place. This coincides with the finding that N_{clu} is one or close to one. In addition, the relatively low value of the parameter n_{hs} arises from the very small aggregation number, and suggests a penetration of the polymer coils of the micelles. This penetration could lead to a slightly larger value of N_{clu} when the coils tend to entangle.

The HMTR polymers with pNiPAm and pDEAm TR blocks have very similar form factor as well as structure factor parameters. The aggregation numbers increased from 5 up to 18 with increasing concentration for both temperatures. Only for **C$_{12}$DMAm$_{127}$NiPAm$_{50}$** and **C$_{12}$DMAm$_{127}$DEAm$_{48}$** at 55 °C, substantially higher aggregation numbers up to 50 and 40 are encountered, respectively. This substantial increase in aggregation explains the marked correlation peak. In that respect, these two polymers behave similar to PEO–PPO–PEO block copolymers (Pluronics) that aggregate and may even form gels upon increasing temperature.[62,63]

The local chain structure remains basically unaffected, as indicated by a constant R_{g} value between 4 nm and 7 nm. The number of clustered micelles is between 1 and 5 at 25°C for the pNiPAm and pDEAm systems, i.e., basically indicating a weak attractive interaction, that increases with increasing TR block length. At the elevated temperature, N_{clu} for the polymers with the shortest TR blocks remains approximately constant. In contrast, the polymers

$C_{12}DMAm_{168}NiPAm_{33}$ and **$C_{12}DMAm_{168}DEAm_{27}$** at 56 °C exhibit cluster sizes of 4–40 micelles in the concentration range of 11–22 g L^{-1}, i.e., here a markedly stronger attraction is seen for the longer LCST blocks. Above this concentration, the cluster sizes decrease below 4 which can be attributed to the closer packing of polymer micelles.

The closer packing is also reflected by the theoretically occupied volume fraction of micelles calculated from the number density of micelles and the total micellar radius. This theoretical volume fraction rises from ~0.3 up to 2.5 where these high values just indicate a marked micellar interpenetration but has no real physical meaning. For the polymers with the longest TR blocks, **$C_{12}DMAm_{127}NiPAm_{50}$** and **$C_{12}DMAm_{127}DEAm_{48}$**, the parameter N_{clu} is mostly below 2 at 55 °C. This means that the attractive interaction is largely increased and leads to a formation of densely packed polymer micelles with a high degree of ordering as indicated by the correlation peak. The values for n_{hs}, which is a measure for the steric repulsion of the polymer corona, are between 0.5 and 1.8. They increase with increasing TR block length, but do not show a pronounced concentration dependency. This observation can be attributed to the growing TR block, which promotes the formation of separate pNiPAm or pDEAm domains.

The pNAP-containing HMTR polymers behave similarly to the hydrophobically modified pDMAm homopolymers **$C_{12}DMAm_{168}$**. The aggregation number rises from ~2 to ~10 with increasing concentration (Figure S24d) where **$C_{12}DMAm_{168}NAP_{27}$** has slightly lower N_{agg} values than **$C_{12}DMAm_{168}NAP_{16}$**, due to the larger hydrophilic group. The fraction of polymer chains in the shell and the radius of gyration are basically concentration independent with values of 2–4 % and ~6 nm, respectively. The polymer **$C_{12}DMAm_{127}NPAm_{31}$** with pNPAm as TR block has a slightly rising aggregation number of about 10 at 25°C and a comparably high value between 30 and 60 at 55 °C. The polymer chain fraction in the shell is close to 5 % at 25 °C, and drops down

to ~0 % at 55 °C. The radius of gyration is slightly smaller compared to the values of the pNAP-based systems, being at 25 °C close to ~4 nm, and at 55°C between 5–7 nm. The reduction of R_g indicates a lower hydration of the pNPAm block. At 25 °C, clustering for **$C_{12}DMAm_{127}NPAm_{31}$** is not very pronounced and similar to **$C_{12}DMAm_{168}NAP_{27}$**. Here it might be noted that this clustering is effectively a measure of attraction between the micellar aggregates. At 55°C and above 20 g L^{-1}, the value of N_{clu} increases from 3 to 5. The penetration of micelles is similar to the pNiPAm- and pDEAm-based systems: the value for n_{hs} is close to 1 at 25 °C, and varies between 1.7 and 1.2 at 55 °C. This reflects the formation of pNPAm domains at 55 °C.

SUMMARY AND CONCLUSIONS

In this work, we studied the self-assembly behavior of BAB* copolymers in aqueous solution. They consist of a short permanently hydrophobic part B of fixed size that bears a *n*-dodecyl chain, a long permanently hydrophilic A block of poly(*N*,*N*-dimethylacrylamide) (pDMAm), and a terminal temperature-responsive (TR) block B* of intermediate length exhibiting an LCST transition. As the permanently hydrophobic part B is part of the R-terminus of the RAFT-made copolymers, it is much less sensitive to cleavage by hydrolysis reactions than the commonly employed hydrophobic groups attached via the Z-terminus. The chemical nature of the B* block was varied by employing different polyacrylamides, i.e., *N*-propylacrylamide (NPAm), *N*-isopropylacrylamide (NiPAm), *N*,*N*-diethylacrylamide (DEAm), and *N*-acryloylpyrrolidine (NAP), which vary with respect to value and type (types I and type II) of their lower critical solution temperature (LCST). The length of the thermo-responsive block as well as that of the pDMAm block were systematically varied, and the aggregation behavior of these BAB* type copolymers was studied as a function of the concentration in the temperature range of 20 to 60 °C.

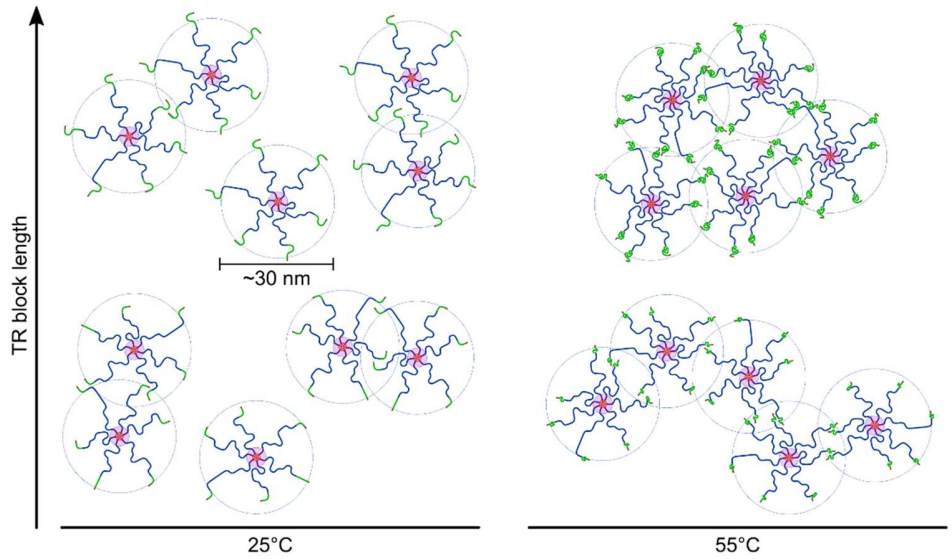

Scheme 4. Schematic description of the temperature-induced changes of self-assembly in the C_{12}-*b*-pDMAm-*b*-TR polymer systems.

As shown by light and neutron scattering (SLS, DLS, SANS), these BAB* polymers form generally small globular aggregates, due to the assembly driven by the permanently hydrophobic end block. The SANS data were analyzed quantitatively via a clustered polymer micelle model, which accounts for the aggregation itself, but also describes the attractive and repulsive interactions that control the self-assembly process. For most systems studied, the temperature-response is relatively small, becoming really significant for more than 20 LCST units, where apparently for the B* block being pNAP and pNPAm, the transition temperature is simply shifted out of the chosen temperature observation window. For the polymers with B* blocks of pNiPAm and pDEAm, an attractive interaction is seen above the effective transition temperature that increases with their block length. Most interestingly, for pNiPAm and pDEAm blocks of ~50 units length, a substantially different aggregation behavior is observed once the LCST is surpassed as followed by SANS and light scattering. At around 35–40 °C, these polymers undergo a very

marked structural transformation, by which compacted and highly ordered hydrophobic domains are formed with an average spacing of ~35–40 nm. Thus, a marked ordering effect is induced upon raising the temperature. Remarkably, this effect is similarly observed in the whole experimental concentration range of 5–60 g L^{-1}, and indicates that the thermo-responsive blocks largely dominate the aggregation behavior.

From all of these observations it can be concluded that by controlling the architecture of the BAB^* copolymers and the choice of the type of the temperature-responsive B^* block, the aggregation behavior can be controlled as a function of temperature. Depending on the choice of the B^* block, one may observe almost no effect upon elevating the temperature, an increased attractive interaction, or the formation of compacted and highly structured aggregates. Accordingly, these systems allow for tailoring the self-assembly response as it might be of interest in a variety of applications, for instance in the fields of cosmetics or delivery systems.

ACKNOWLEDGEMENTS

We thank the *Deutsche Forschungsgemeinschaft* (DFG) for financially supporting this work (grants GR 1030/22-1 and LA 611/17-19). For granting and financially supporting neutron scattering beamtimes, we gratefully acknowledge the *Heinz Maier–Leibnitz Zentrum* (MLZ) in cooperation with the *Forschungszentrum Jülich GmbH* (Proposal 14026), *Institut Laue–Langevin* (ILL, Proposal 9-12-545 [64]), and ISIS Pulsed Neutron Source (STFC Rutherford Appleton Laboratory, Didcot, U.K.). We also thank Sascha Prenzel and Helmut Schlaad (Universität Potsdam) for support by SEC analysis, and Jana Lutzki (TU Berlin) for measuring refractive index increments of the polymers.

ASSOCIATED CONTENT

Supporting Information

The document with the Supporting Information (SI, provided as PDF file) includes additional information about chemicals and their syntheses, all used data sets, and further details of the data analyses.

AUTHOR INFORMATION

Corresponding Author

* Prof. Michael Gradzielski, E-mail: michael.gradzielski@tu-berlin.de, Address: Technische Universität Berlin, Department of Chemistry, TC7, Strasse des 17. Juni 124, 10623 Berlin, Germany; orcid.org/0000-0002-7262-7115

* Prof. André Laschewsky, E-mail: laschews@uni-potsdam.de, Address: Universität Potsdam, Department of Chemistry, Angewandte Polymerchemie, Karl-Liebknecht-Strasse 24-25, 14476 Potsdam, Germany; orcid.org/0000-0003-2443-886X

Present Addresses

† Federal Police Special Operations Command 11, Section 13, Schöneberger Strasse 14/15, 10963 Berlin, Germany

Author Contributions

The manuscript was written through contributions of the authors Albert Prause‡, Michelle Hechenbichler‡, André Laschewsky, and Michael Gradzielski. Benjamin von Lospichl was measuring the SANS data at KWS-1. Artem Feoktystov, Ralf Schweins, and Najet Mahmoudi

were the local contacts at the SANS instruments KWS-1, D33, and ZOOM, respectively. All authors have given approval to the final version of the manuscript.

‡These authors contributed equally.

Funding Sources

This work was supported by *Deutsche Forschungsgemeinschaft* (DFG), grants GR 1030/22-1 and LA 611/17-1. The small angle neutron scattering beamtimes were granted and founded by *Heinz Maier–Leibnitz Zentrum* (MLZ) in cooperation with the *Forschungszentrum Jülich GmbH*, *Institut Laue–Langevin* (ILL),[64] and ISIS Pulsed Neutron Source (STFC Rutherford Appleton Laboratory, Didcot, U.K.).

REFERENCES

(1) Brassinne, J.; Zhuge, F.; Fustin, C. A.; Gohy, J. F. Precise Control over the Rheological Behavior of Associating Stimuli-Responsive Block Copolymer Gels. *Gels* **2015**, *1* (2), 235–255. https://doi.org/10.3390/gels1020235.

(2) Raffa, P.; Wever, D. A. Z.; Picchioni, F.; Broekhuis, A. A. Polymeric Surfactants: Synthesis, Properties, and Links to Applications. *Chem. Rev.* **2015**, *115* (16), 8504–8563. https://doi.org/10.1021/cr500129h.

(3) Karayianni, M.; Pispas, S. Journal of Polymer Science - 2021 - Karayianni - Block Copolymer Solution Self-assembly Recent Advances Emerging Trends .Pdf. *J. Polym. Sci.* **2021**, *59*, 1874–1898.

(4) Cabral, H.; Miyata, K.; Osada, K.; Kataoka, K. Block Copolymer Micelles in Nanomedicine Applications. *Chem. Rev.* **2018**, *118* (14), 6844–6892. https://doi.org/10.1021/acs.chemrev.8b00199.

(5) Strandman, S.; Zhu, X. X. Thermo-Responsive Block Copolymers with Multiple Phase Transition Temperatures in Aqueous Solutions. *Prog. Polym. Sci.* **2015**, *42*, 154–176. https://doi.org/10.1016/j.progpolymsci.2014.10.008.

(6) Papadakis, C. M.; Müller-Buschbaum, P.; Laschewsky, A. Switch It Inside-out: "Schizophrenic" Behavior of All Thermoresponsive UCST-LCST Diblock Copolymers. *Langmuir* **2019**, *35* (30), 9660–9676. https://doi.org/10.1021/acs.langmuir.9b01444.

(7) Halperin, A.; Kröger, M.; Winnik, F. M. Poly(N-Isopropylacrylamide) Phase Diagrams: Fifty Years of Research. *Angew. Chemie - Int. Ed.* **2015**, *54* (51), 15342–15367.

https://doi.org/10.1002/anie.201506663.

(8) Luo, G. F.; Chen, W. H.; Zhang, X. Z. 100th Anniversary of Macromolecular Science Viewpoint: Poly(N-Isopropylacrylamide)-Based Thermally Responsive Micelles. *ACS Macro Lett.* **2020**, *9* (6), 872–881. https://doi.org/10.1021/acsmacrolett.0c00342.

(9) Heskins, M.; Guillet, J. E. Solution Properties of Poly(N-Isopropylacrylamide). *J. Macromol. Sci. Part A - Chem.* **1968**, *2* (8), 1441–1455. https://doi.org/10.1080/10601326808051910.

(10) Platé, N. A.; Lebedeva, T. L.; Valuev, L. I. Lower Critical Solution Temperature in Aqueous Solutions of N-Alkyl-Substituted Polyacrylamides. *Polym. J.* **1999**, *31* (1), 21–27. https://doi.org/10.1295/polymj.31.21.

(11) Aseyev, V.; Tenhu, H.; Winnik, F. M. Non-Ionic Thermoresponsive Polymers in Water. *Adv. Polym. Sci.* **2011**, *242* (1), 29–89. https://doi.org/10.1007/12_2010_57.

(12) Gradzielski, M.; Rauscher, A.; Hoffmann, H. Hydrophobically Cross-Linked Micellar Solutions: Microstructure and Properties of the Solutions. *J. Phys. IV* **1993**, *3 (C1)* (1), 65–79. https://doi.org/10.1051/jp4:1993107.

(13) Molino, F.; Appell, J.; Filali, M.; Michel, E.; Porte, G.; Mora, S.; Sunyer, E. A Transient Network of Telechelic Polymers and Microspheres: Structure and Rheology. *J. Phys. Condens. Matter* **2000**, *12* (8A), A491–A498. https://doi.org/10.1088/0953-8984/12/8A/368.

(14) Herfurth, C.; Malo de Molina, P.; Wieland, C.; Rogers, S.; Gradzielski, M.; Laschewsky, A. One-Step RAFT Synthesis of Well-Defined Amphiphilic Star Polymers and Their Self-

Assembly in Aqueous Solution. *Polym. Chem.* **2012**, *3* (6), 1606–1617. https://doi.org/10.1039/c2py20126g.

(15) Malo de Molina, P.; Ihlefeldt, F. S.; Prévost, S.; Herfurth, C.; Appavou, M. S.; Laschewsky, A.; Gradzielski, M. Phase Behavior of Nonionic Microemulsions with Multi-End-Capped Polymers and Its Relation to the Mesoscopic Structure. *Langmuir* **2015**, *31* (18), 5198–5209. https://doi.org/10.1021/acs.langmuir.5b00817.

(16) Herfurth, C.; Voll, D.; Buller, J.; Weiss, J.; Barner-Kowollik, C.; Laschewsky, A. Radical Addition Fragmentation Chain Transfer (RAFT) Polymerization of Ferrocenyl (Meth)Acrylates. *J. Polym. Sci. Part A Polym. Chem.* **2012**, *50* (1), 108–118. https://doi.org/10.1002/pola.24994.

(17) Herfurth, C.; Laschewsky, A.; Noirez, L.; von Lospichl, B.; Gradzielski, M. Thermoresponsive (Star) Block Copolymers from One-Pot Sequential RAFT Polymerizations and Their Self-Assembly in Aqueous Solution. *Polymer* **2016**, *107*, 422–433. https://doi.org/10.1016/j.polymer.2016.09.089.

(18) Fischer, F.; Zufferey, D.; Tahoces, R. Lower Critical Solution Temperature in Superheated Water: The Highest in the Poly(N,N-Dialkylacrylamide) Series. *Polym. Int.* **2011**, *60* (8), 1259–1262. https://doi.org/10.1002/pi.3071.

(19) Hechenbichler, M.; Laschewsky, A.; Gradzielski, M. Poly(N,N-Bis(2-Methoxyethyl)Acrylamide), a Thermoresponsive Non-Ionic Polymer Combining the Amide and the Ethyleneglycolether Motifs. *Colloid Polym. Sci.* **2021**, *299* (2), 205–219. https://doi.org/10.1007/s00396-020-04701-9.

(20) Ito, S. Phase Transition of Aqueous Solution of Poly(N-Alkylacrylamide) Derivatives - Effects of Side Chain Structures. *Kobunshi Ronbunshu* **1989**, *46* (7), 437–443. https://doi.org/10.1295/koron.46.437.

(21) Ulbrich, K.; Kopeček, J. Cross-Linked Copolymers of N,N-Diethylacrylamide with Improved Mechanical Properties. **1979**, *66*, 209–219. https://doi.org/10.1002/polc.5070660122.

(22) Skrabania, K.; Kristen, J.; Laschewsky, A.; Akdemir, Ö.; Hoth, A.; Lutz, J. F. Design, Synthesis, and Aqueous Aggregation Behavior of Nonionic Single and Multiple Thermoresponsive Polymers. *Langmuir* **2007**, *23* (1), 84–93. https://doi.org/10.1021/la061509w.

(23) Lang, X.; Patrick, A. D.; Hammouda, B.; Hore, M. J. A. Chain Terminal Group Leads to Distinct Thermoresponsive Behaviors of Linear PNIPAM and Polymer Analogs. *Polymer* **2018**, *145*, 137–147. https://doi.org/10.1016/j.polymer.2018.04.068.

(24) Eggers, S.; Eckert, T.; Abetz, V. Double Thermoresponsive Block–Random Copolymers with Adjustable Phase Transition Temperatures: From Block-like to Gradient-like Behavior. *J. Polym. Sci. Part A Polym. Chem.* **2018**, *56* (4), 399–411. https://doi.org/10.1002/pola.28906.

(25) Skrabania, K.; Miasnikova, A.; Bivigou-Koumba, A. M.; Zehm, D.; Laschewsky, A. Examining the UV-Vis Absorption of RAFT Chain Transfer Agents and Their Use for Polymer Analysis. *Polym. Chem.* **2011**, *2* (9), 2074–2083. https://doi.org/10.1039/c1py00173f.

(26) Wu, H. Correlations between the Rayleigh Ratio and the Wavelength for Toluene and Benzene. *Chem. Phys.* **2010**, *367* (1), 44–47. https://doi.org/10.1016/j.chemphys.2009.10.019.

(27) Schnablegger, H.; Glatter, O. Optical Sizing of Small Colloidal Particles: An Optimized Regularization Technique. *Appl. Opt.* **1991**, *30* (33), 4889. https://doi.org/10.1364/ao.30.004889.

(28) Schnablegger, H.; Glatter, O. Simultaneous Determination of Size Distribution and Refractive Index of Colloidal Particles from Static Light-Scattering Experiments. *J. Colloid Interface Sci.* **1993**, *158* (1), 228–242. https://doi.org/10.1006/jcis.1993.1250.

(29) Prause, A. SimplightQt https://git.tu-berlin.de/MolMat/SimplightQt (accessed Apr 28, 2022).

(30) Frielinghaus, H.; Feoktystov, A.; Berts, I.; Mangiapia, G. KWS-1: Small-Angle Scattering Diffractometer. *J. large-scale Res. Facil. JLSRF* **2015**, *1*, 26–29. https://doi.org/10.17815/jlsrf-1-26.

(31) Feoktystov, A. V.; Frielinghaus, H.; Di, Z.; Jaksch, S.; Pipich, V.; Appavou, M. S.; Babcock, E.; Hanslik, R.; Engels, R.; Kemmerling, G.; Kleines, H.; Ioffe, A.; Richter, D.; Brückel, T. KWS-1 High-Resolution Small-Angle Neutron Scattering Instrument at JCNS: Current State. *J. Appl. Crystallogr.* **2015**, *48* (1), 61–70. https://doi.org/10.1107/S1600576714025977.

(32) Dewhurst, C. D. D33 - A Third Small-Angle Neutron Scattering Instrument at the Institut Laue Langevin. *Meas. Sci. Technol.* **2008**, *19* (3). https://doi.org/10.1088/0957-

0233/19/3/034007.

(33) STFC Rutherford Appleton Laboratory. ISIS Pulsed Neutron Source https://www.isis.stfc.ac.uk (accessed Apr 28, 2022).

(34) Pipich, V. QtiSAS: user-friendly program for reduction, visualization, analysis and fit of SA(N)S data http://www.qtisas.com (accessed Apr 28, 2022).

(35) Richard, D.; Ferrand, M.; Kearley, G. J. Analysis and Visualisation of Neutron-Scattering Data. *J. Neutron Res.* **1996**, *4* (1–4), 33–39. https://doi.org/10.1080/10238169608200065.

(36) Arnold, O.; Bilheux, J. C.; Borreguero, J. M.; Buts, A.; Campbell, S. I.; Chapon, L.; Doucet, M.; Draper, N.; Ferraz Leal, R.; Gigg, M. A.; Lynch, V. E.; Markvardsen, A.; Mikkelson, D. J.; Mikkelson, R. L.; Miller, R.; Palmen, K.; Parker, P.; Passos, G.; Perring, T. G.; Peterson, P. F.; Ren, S.; Reuter, M. A.; Savici, A. T.; Taylor, J. W.; Taylor, R. J.; Tolchenov, R.; Zhou, W.; Zikovsky, J. Mantid - Data Analysis and Visualization Package for Neutron Scattering and μ SR Experiments. *Nucl. Instruments Methods Phys. Res. Sect. A Accel. Spectrometers, Detect. Assoc. Equip.* **2014**, *764*, 156–166. https://doi.org/10.1016/j.nima.2014.07.029.

(37) Hammouda, B. SANS from Homogeneous Polymer Mixtures: A Unified Overview. In *Polymer Characteristics*; Springer Berlin Heidelberg: Berlin, Heidelberg, 1993; pp 87–133. https://doi.org/10.1007/BFb0025862.

(38) Zinn, T.; Willner, L.; Knudsen, K. D.; Lund, R. Self-Assembly of Mixtures of Telechelic and Monofunctional Amphiphilic Polymers in Water: From Clusters to Flowerlike Micelles. *Macromolecules* **2017**, *50* (18), 7321–7332.

https://doi.org/10.1021/acs.macromol.7b01501.

(39) Wei, Y.; Hore, M. J. A. Characterizing Polymer Structure with Small-Angle Neutron Scattering: A Tutorial. *J. Appl. Phys.* **2021**, *129* (17). https://doi.org/10.1063/5.0045841.

(40) Hammouda, B.; Kim, M. H. The Empirical Core-Chain Model. *J. Mol. Liq.* **2017**, *247*, 434–440. https://doi.org/10.1016/j.molliq.2017.09.114.

(41) Schweins, R.; Huber, K. Particle Scattering Factor of Pearl Necklace Chains. *Macromol. Symp.* **2004**, *211*, 25–42. https://doi.org/10.1002/masy.200450702.

(42) Prause, A.; Hörmann, A.; Cristiglio, V.; Smales, G. J.; Thünemann, A. F.; Gradzielski, M.; Findenegg, G. H. Incorporation and Structural Arrangement of Microemulsion Droplets in Cylindrical Pores of Mesoporous Silica. *Mol. Phys.* **2021**, *119* (15–16), e1913255. https://doi.org/10.1080/00268976.2021.1913255.

(43) Pedersen, J. S.; Gerstenberg, M. C. Scattering Form Factor of Block Copolymer Micelles. *Macromolecules* **1996**, *29* (4), 1363–1365. https://doi.org/10.1021/ma9512115.

(44) Burchard, W.; Kajiwara, K. The Statistics of Stiff Chain Molecules I. The Particle Scattering Factor. *Proc. R. Soc. London Ser. A* **1970**, *316* (1525), 185–199.

(45) Kinning, D. J.; Thomas, E. L. Hard-Sphere Interactions Between Spherical Domains in Diblock Copolymers. *Macromolecules* **1984**, *17* (9), 1712–1718. https://doi.org/10.1021/ma00139a013.

(46) Paulin, S. E.; Ackerson, B. J. Observation of a Phase Transition in the Sedimentation Velocity of Hard Spheres. *Phys. Rev. Lett.* **1990**, *64* (22), 2663–2666. https://doi.org/10.1103/PhysRevLett.64.2663.

(47) Perrier, S. 50th Anniversary Perspective: RAFT Polymerization - A User Guide. *Macromolecules* **2017**, *50* (19), 7433–7447. https://doi.org/10.1021/acs.macromol.7b00767.

(48) Samakande, A.; Chaghi, R.; Derrien, G.; Charnay, C.; Hartmann, P. C. Aqueous Behaviour of Cationic Surfactants Containing a Cleavable Group. *J. Colloid Interface Sci.* **2008**, *320* (1), 315–320. https://doi.org/10.1016/j.jcis.2008.01.022.

(49) Rieger, J.; Osterwinter, G.; Bui, C.; Stoffelbach, F.; Charleux, B. Surfactant-Free Controlled/Living Radical Emulsion (Co)Polymerization of n-Butyl Acrylate and Methyl Methacrylate via RAFT Using Amphiphilic Polyethylene Oxide-Based Trithiocarbonate Chain Transfer Agents. *Macromolecules* **2009**, *42* (15), 5518–5525. https://doi.org/10.1021/ma9008803.

(50) Mertoglu, M.; Laschewsky, A.; Skrabania, K.; Wieland, C. New Water Soluble Agents for Reversible Addition-Fragmentation Chain Transfer Polymerization and Their Application in Aqueous Solutions. *Macromolecules* **2005**, *38* (9), 3601–3614. https://doi.org/10.1021/ma048268o.

(51) Päch, M.; Zehm, D.; Lange, M.; Dambowsky, I.; Weiss, J.; Laschewsky, A. Universal Polymer Analysis by 1H NMR Using Complementary Trimethylsilyl End Groups. *J. Am. Chem. Soc.* **2010**, *132* (25), 8757–8765. https://doi.org/10.1021/ja102096u.

(52) Weiss, J.; Böttcher, C.; Laschewsky, A. Self-Assembly of Double Thermoresponsive Block Copolymers End-Capped with Complementary Trimethylsilyl Groups. *Soft Matter* **2011**, *7* (2), 483–492. https://doi.org/10.1039/c0sm00531b.

(53) Liu, H. Y.; Zhu, X. X. Lower Critical Solution Temperatures of N-Substituted Acrylamide Copolymers in Aqueous Solutions. *Polymer* **1999**, *40* (25), 6985–6990. https://doi.org/10.1016/S0032-3861(98)00858-1.

(54) Miasnikova, A.; Laschewsky, A.; De Paoli, G.; Papadakis, C. M.; Müller-Buschbaum, P.; Funari, S. S. Thermoresponsive Hydrogels from Symmetrical Triblock Copolymers Poly(Styrene-Block-(Methoxy Diethylene Glycol Acrylate)-Block-Styrene). *Langmuir* **2012**, *28* (9), 4479–4490. https://doi.org/10.1021/la204665q.

(55) Skrabania, K.; Li, W.; Laschewsky, A. Synthesis of Double-Hydrophilic BAB Triblock Copolymers via RAFT Polymerisation and Their Thermoresponsive Self-Assembly in Water. *Macromol. Chem. Phys.* **2008**, *209* (13), 1389–1403. https://doi.org/10.1002/macp.200800108.

(56) Convertine, A. J.; Lokitz, B. S.; Vasileva, Y.; Myrick, L. J.; Scales, C. W.; Lowe, A. B.; McCormick, C. L. Direct Synthesis of Thermally Responsive DMA/NIPAM Diblock and DMA/NIPAM/DMA Triblock Copolymers via Aqueous, Room Temperature RAFT Polymerization. *Macromolecules* **2006**, *39* (5), 1724–1730. https://doi.org/10.1021/ma0523419.

(57) Kujawa, P.; Segui, F.; Shaban, S.; Diab, C.; Okada, Y.; Tanaka, F.; Winnik, F. M. Impact of End-Group Association and Main-Chain Hydration on the Thermosensitive Properties of Hydrophobically Modified Telechelic Poly(N-Isopropylacrylamides) in Water. *Macromolecules* **2006**, *39* (1), 341–348. https://doi.org/10.1021/ma051876z.

(58) Bivigou-Koumba, A. M.; Kristen, J.; Laschewsky, A.; Müller-Buschbaum, P.; Papadakis, C. M. Synthesis of Symmetrical Triblock Copolymers of Styrene and N-

Isopropylacrylamide Using Bifunctional Bis(Trithiocarbonate)s as RAFT Agents. *Macromol. Chem. Phys.* **2009**, *210* (7), 565–578. https://doi.org/10.1002/macp.200800575.

(59) Inomata, H.; Goto, S.; Saito, S. Phase Transition of N-Substituted Acrylamide Gels. *Macromolecules* **1990**, *23* (22), 4887–4888. https://doi.org/10.1021/ma00224a023.

(60) Cheng, H.; Shen, L.; Wu, C. LLS and FTIR Studies on the Hysteresis in Association and Dissociation of Poly(N-Isopropylacrylamide) Chains in Water. *Macromolecules* **2006**, *39* (6), 2325–2329. https://doi.org/10.1021/ma052561m.

(61) Hammouda, B. SANS from Polymers-Review of the Recent Literature. *Polym. Rev.* **2010**, *50* (1), 14–39. https://doi.org/10.1080/15583720903503460.

(62) Hecht, E.; Mortensen, K.; Hoffmann, H. L3 Phase in a Binary Block Copolymer/Water System. *Macromolecules* **1995**, *28*, 5465–5476. https://doi.org/10.1021/ma00120a010.

(63) Mortensen, K.; Talmon, Y. Cryo-TEM and SANS Microstructural Study of Pluronic Polymer Solutions. *Macromolecules* **1995**, *28* (26), 8829–8834. https://doi.org/10.1021/ma00130a016.

(64) Bayer, S.; Prause, A.; Azeri, O.; Simon, M.; Schweins, R.; Gradzielski, M. *Tuning Electrostatic Interactions in Uncommon Structures in Hyaluronate/Surfactant Complexes*; Grenoble, 2019. https://doi.org/10.5291/ILL-DATA.9-12-545.

(65) Shirota, H.; Kuwabara, N.; Ohkawa, K.; Horie, K. Deuterium Isotope Effect on Volume Phase Transition of Polymer Gel: Temperature Dependence. *J. Phys. Chem. B* **1999**, *103* (47), 10400–10408. https://doi.org/10.1021/jp992401a.

(66) Mao, H.; Li, C.; Zhang, Y.; Furyk, S.; Cremer, P. S.; Bergbreiter, D. E. High-Throughput

Studies of the Effects of Polymer Structure and Solution Components on the Phase Separation of Thermoresponsive Polymers. *Macromolecules* **2004**, *37* (3), 1031–1036. https://doi.org/10.1021/ma035590a.